学位論文

Studies of temperature-pressure paths of the Sambagawa metamorphism

三波川変成作用の温度圧力経路の研究

平成11年12月博士（理学）申請

東京大学大学院理学系研究科
地質学専攻

林（能）睦子

学 位 論 文

Studies of temperature-pressure paths of the Sambagawa metamorphism

三波川変成作用の温度圧力経路の研究

平成 11 年　12 月　博士（理学）申請

東京大学大学院理学系研究科
地質学専攻

林（乾）睦子

Contents

Introduction

Metamorphic rocks are the scarce evidences of earth's dynamic activity that is real and tangible. Rocks are metamorphosed in solid state, preserving their original configuration in large scale. Yet in small scale, they gradually deform and recrystallize in response to changing environment, that what we see in those rocks today are the mixtures of various indices and records. Metamorphic rocks provide abundant informations concerning conditions they went through, only if the time sequence is appropriately unraveled.

The Sambagawa metamorphic belt in south-western Japan is a high pressure intermediate type metamorphic belt mainly composed of rocks of sedimentary origin, presumably once drawn into the earth by the subducting lithosphere underneath. It is regarded as one of the typical regional metamorphic belts created by subduction tectonics. History of changing condition and dynamic flow that lead to present state of Sambagawa schists provides a significant constraint onto the mechanism of plate subduction.

In Besshi district, central Shikoku, there are some exotic rock masses present among schists of highest grade. Those tectonic blocks, with the largest Iratsu mass measuring up to 7 km long, are identified as being metamorphosed gabbro and ultramafic rocks (Kunugiza et al., 1986). They have different and complex histories before being incorporated into the Sambagawa schists sometime before or during peak temperature stage. It seems natural that these rock masses and surrounding schists were both deformed by some large-scale solid-state flow relevant to subduction tectonics. It is essential to know the static and dynamic conditions at the time of their emplacement to unravel the dominant tectonics.

There are, however, several contrasting models about the emplacement of even a single rock mass. Takasu (1986) suggested pelitic schists in contact with one of the small metagabbro bodies were subject to contact metamorphism due to the emplacement of supposed hot rock mass. Aoya (1998), on the other hand, argued that it is unreasonable for a solid-state displacement of such a rock body to cause contact aureole of certain width, unless they are implausibly large. If this is true, the observed high temperature metamorphism must be caused by a regional event. In any case, the key evidence would be recorded as some kind of disturbance to the surrounding schists as the result of the emplacement.

Detailed pressure-temperature history of individual rock will greatly help to set constraint onto the timing and circumstance of the emplacement. The Sambagawa metamorphic belt has been extensively investigated (review in Wallis and Banno, 1990), including the efforts to determine P-T conditions of metamorphism. Along with estimation of peak metamorphic temperatures, it has been made clear that rocks from different metamorphic grade record different P-T paths, based on chemical zoning of minerals. Garnet is known for its potential ability to record the time series of changing pressure and temperature condition as chemical zoning (Spear, 1993). Many previous studies of the Sambagawa belt estimated P-T conditions from chemical zonings of garnet (Banno et al., 1986; Takasu, 1986; Toriumi and Kohsaka, 1994; Enami, 1998). Most of those studies concern either to the Sambagawa schists or to the exotic rock masses themselves. It is known that various zoning patterns of garnet are characteristically found in the schists in contact with the tectonic blocks. However, no quantitative consideration has ever been given to this

suspected record of the disturbance.

In this study, time series of garnet growth is unraveled for pelitic schists at the periphery of the Iratsu metagabbro. The record of thermal and tectonic disturbance caused by the emplacement is distinguished from the common pattern of growth due to the Sambagawa regional metamorphism. Suspected non-equilibrium growth is also investigated in detail to define the time of their occurrences. Pressure and temperature histories for normal and disturbed growths of garnet were calculated quantitatively using differential thermodynamic method. Garnet has been widely used for analysis of metamorphic condition, that there are plenty of thermodynamic data required for quantitative calculation.

The Sambagawa metamorphic belt has a long history of petrological and geological investigations, that the deduced P-T history can be examined within the frame of previously established stories. Also on the contrary, a new insight is acquired for the tectonic process of the Sambagawa metamorphic belt based on the newly derived P-T history.

1. Geologic setting

1-1. Metamorphic zonal structure

The Sambagawa metamorphic belt, which extends for around 800 km, is a high-pressure intermediate type metamorphic belt in the Outer Belt of the southwest Japan. To the north it borders on the Ryoke high-temperature metamorphic belt, the boundary provided by a major fault zone called the Median Tectonic Line. To the south lies the northern Chichibu belt.

Central Shikoku is where the Sambagawa metamorphic belt is exposed in the largest extent, around 30 km in width. The highest grade schists occur in central Shikoku. The Sambagawa metamorphic rocks here consist mainly of pelitic schists accompanied with basic schists. Minor amounts of quartz schists and psammitic schists are found, but calcareous schists are rare.

Lithological structure of the Sambagawa metamorphic belt has been traditionally defined in central Shikoku as the Ojoin Formation, the Minawa Formation (the Upper, Main, and Lower Members), the Koboke Formation, and the Kawaguchi Formation in the descending order (Kojima et al., 1956; Higashino, 1990). The Ojoin Formation is mainly pelitic and psammitic rocks. The Upper Member of the Minawa Formation is predominantly composed of pelitic, basic, and quartz schists. The Main and the Lower Members of the Minawa Formation comprises basic schists and pelitic schists, respectively. The formation boundaries are superposed on the metamorphic zonal map (fig.1-1).

Metamorphic zonation has been defined by mineral assemblages in pelitic rocks: the chlorite zone (C), the garnet zone (G), the albite-biotite zone (AB), and the oligoclase-biotite zone (OB), in the order of increasing metamorphic temperature (fig.1-1) (Higashino, 1990). The chlorite zone has

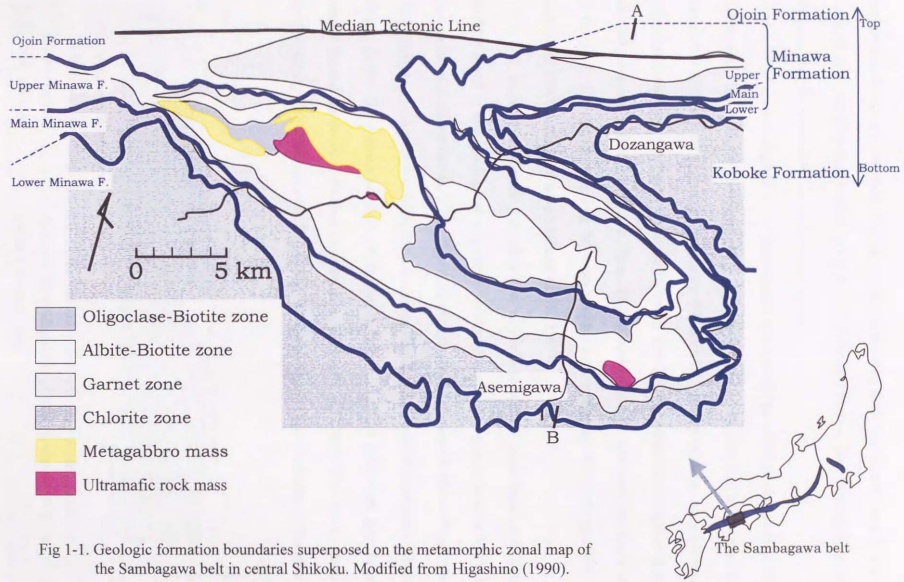

Fig 1-1. Geologic formation boundaries superposed on the metamorphic zonal map of the Sambagawa belt in central Shikoku. Modified from Higashino (1990).

experienced the greenschist facies metamorphism, and the above two biotite zones have reached the higher epidote-amphibolite facies. The petrographical feature will be described in the next chapter.

The metamorphic zone boundaries are nearly parallel to the geological bandings. The geologic strata slightly dip northward to expose the top layers in the north. The whole structure is gently folded with nearly vertical axis planes, their half wavelength being around 10 to 15 km. The syncline is recognized as the large scale inflection of the formation boundaries in the eastern part of figure 1-1. The gentle folding belongs to the last stage of the deformational history of the Sambagawa belt (Hara et al., 1990).

It is seen in figure 1-1, that the oligoclase-biotite zone locates at the middle level of the geological sequence, and metamorphic grade descends both upwards and downwards. This thermal structure is observed throughout the Sambagawa metamorphic belt, from eastern Kyushu to Kanto Mountains (Hara et al., 1990). The cross-section of the metamorphic zonal structure has been drawn based on several drilled core studies (Higashino, 1990). The north-south profile along the Asemigawa River (fig.1-2) confirms that the entire thermal

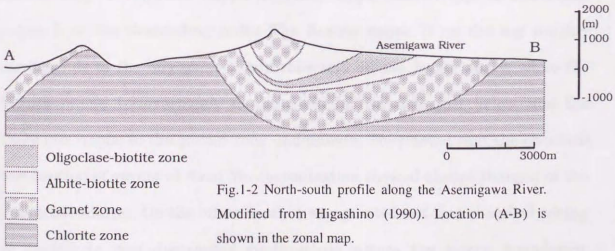

Fig.1-2 North-south profile along the Asemigawa River. Modified from Higashino (1990). Location (A-B) is shown in the zonal map.

structure with the highest grade in the middle has been completed before the last synclinal deformation.

There are two extremely different models proposed as the mechanism to form the observed thermal structure. It is supposed that there is a large south vergent recumbent fold that made the highest grade layer place in the middle, on the assumption that the whole Sambagawa sequence acted as a continuous geological body (e.g., Banno et al., 1978; Toriumi, 1985; Otsuki, 1992; Wallis 1998). Chemical index of temperature, namely the Fe-Mg distribution coefficients between garnet and chlorite, provides the support for this continuous model. The distribution coefficients show smooth changes from one metamorphic zone to another, indicating the structure to be synmetamorphic (Higashino, 1990).

In contrast, other workers suppose that the inverted thermal structure was created as a result of several nappes piled up during exhumation (e.g., Faure, 1985; Hara et al., 1990). Piled nappe structure requires discontinuity in the thermal structure. Hara et al. (1990) argued that the Sambagawa metamorphic belt in central Shikoku consists of six nappes: Saruta nappe II, Saruta nappe I, Fuyunose nappe, Sogauchi nappe, Oboke nappe II, and Oboke nappe I, in the descending order. The Saruta nappe II on the top roughly corresponds to the oligoclase-biotite zone and all the layers above, while the Saruta nappe I corresponds to the albite-biotite zone just below, and the Fuyunose nappe to the garnet zone underneath. They noted that the chemical composition of garnet at fixed Mn concentration showed abrupt changes at the nappe boundaries. On the other hand, it was pointed out that chemical zoning of amphibole was distributed continuously across the nappe boundaries.

Chemical zoning in amphibole is known to form mostly during the retrograde stage. Hara et al. (1990) suggested that the nappe structure was formed during or just after the peak metamorphism. Amphiboles were thus able to record the structural condition at the peak metamorphism as the various zoning types.

East-west mineral lineations are developed rather concordantly throughout the Sambagawa metamorphic belt. The foliations are generally dipping northward. The shear sense is commonly top to the west. Supposed plate motion at the time of Sambagawa metamorphism is rapid northward subduction of the Izanagi oceanic plate under the East-Asian continental margin. This highly oblique convergence is consistent with the shear sense and the east-west elongation of the Sambagawa metamorphic belt (Wallis, 1998).

1-2. Tectonic blocks

Many tectonic blocks occur in the albite- and oligoclase-biotite zones (review in Kunugiza et al., 1986). Most of them are found within the Upper Member of the Minawa Formation, which roughly fall into the Saruta nappe I according to the definition of Hara (1990). The tectonic blocks are found as concordant lenticular rock masses. They measure from several tens of meters up to several kilometers in length. Bulk chemical composition is either mafic or ultramafic. Their complex history lead to the concept that it was a part of a mélange zone.

It has been found out that the history of those tectonic blocks before emplacement into the Sambagawa belt is not at all uniform. First, there are rocks with sedimentary origin that were progressively brought into the eclogite facies metamorphism. Second, there are ultramafic and gabbroic cumulate rock

masses that only retain retrograde P-T change from the eclogite into the epidote-amphibolite facies (Kunugiza et al., 1986; Takasu et al., 1994).

Some of the mafic rock bodies show clear bandings that helped themselves identified as metamorphosed layered gabbro (Banno et al., 1976), including the eastern part of the Iratsu mass with the exposed area of 3 x 7 km at ground surface. The Iratsu mass mainly consists of garnet-clinozoisite amphibolite and eclogite, and evidence of prograde metamorphism under the condition of the Sambagawa metamorphism (the epidote-amphibolite facies) is not observed. It is now considered as two different rock masses. The western part of the Iratsu mass is probably of sedimentary origin. The eastern part exhibits typical gabbroic layering texture.

Mineral lineation at the inner part of the eastern and the western Iratsu mass is highly oblique to the dominant east-west flow structure of the Sambagawa belt (Toriumi and Kohsaka, 1994). However, it was found out that the lineation near the boundary was nearly concordant to the host pelitic schists. It confirms the exotic origin of the tectonic block. It is also indicated that the rock mass was emplaced into the Sambagawa schists before the current schistosity was formed.

1-3. Besshi area

Samples for this study were taken mainly from the periphery of the tectonic blocks distributed in Besshi area, along the Dozangawa River (fig.1-3). The area corresponds to the Upper Member of the Minawa Formation as described before.

Pelitic schists of the albite-biotite zone are dominant in the area,

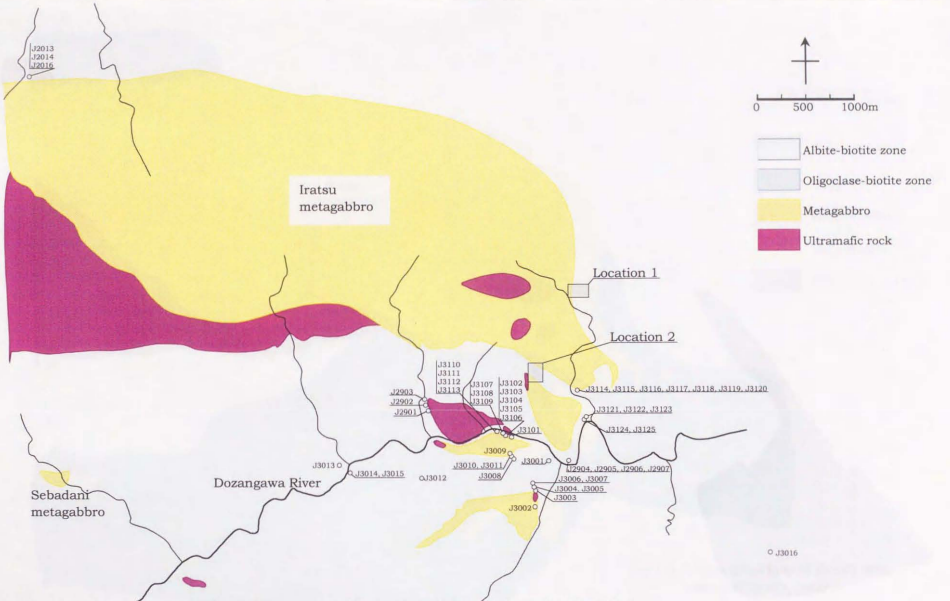

Fig 1-3. Metamorphic zonal map of Besshi area, central Shikoku, Japan. Modified from Higashino (1990).
○: Sample locations and sample numbers. Sample numbers for "location 1" and "2" are depicted separately.

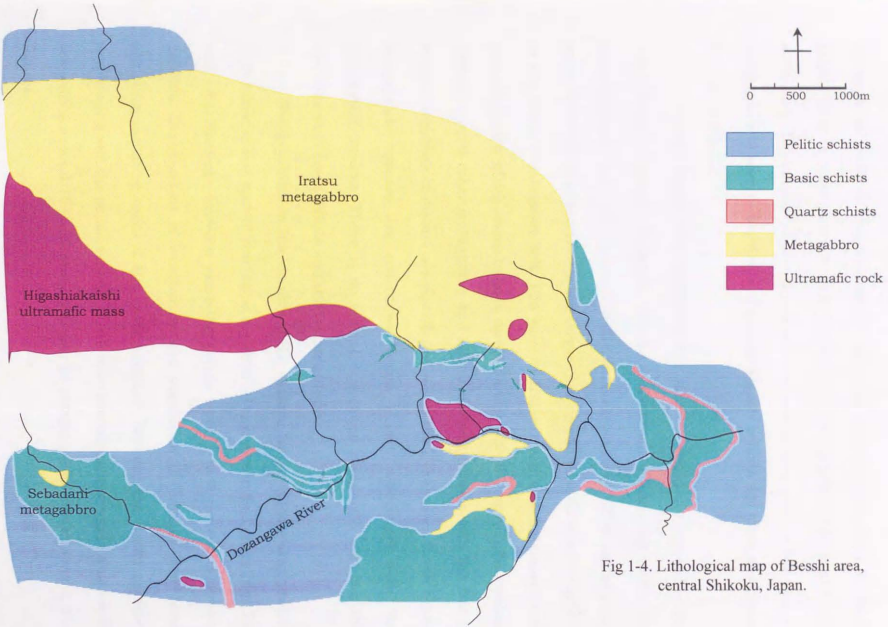

Fig 1-4. Lithological map of Besshi area, central Shikoku, Japan.

accompanied with smaller amount of basic and quartz schists (fig.1-4). Basic schists seem to occur as layers or in lenticular shapes, nearly concordant to the schistosity. Thicknesses of the layers of basic schists vary from a few tens of centimeters to several hundreds of meters. Quartz schists are often associated with basic schists.

Tectonic blocks with ultramafic and gabbroic origin are exposed in the area, having various elongated shapes but mostly concordant with the dominant east-west flow structure of the Sambagawa schists. The eastern and western Iratsu mass together is the largest among the tectonic blocks exposed in the whole Sambagawa belt. The eastern Iratsu mass is a metamorphosed layered gabbro, which seems to be in direct contact with the surrounding pelitic schists. Several other metagabbro and ultramafic rock masses with the size of several hundreds of meters are distributed along the Dozangawa River. Small serpentinite masses are sometimes found closely associated with the metagabbro masses. There is no spatial correlation recognized between the distribution of basic schists and the tectonic blocks.

Pelitic schists in the vicinity of the eastern Iratsu epidote-amphibolite were taken in fine spatial resolution for detailed analyses in this study (figs.1-5 and 1-6). Spacings between sampling points were 1 to 5 meters, wherever possible. Development of weathering and vegetation in patches obstructed sampling, including rocks at the exact boundary between the Iratsu epidote-amphibolite and the pelitic schists. There were several unobservable zones with the widths around 10 to 20 meters as can be recognized as blank areas in the figures.

Basic schists occurred probably as layers or lenticular bodies, with the

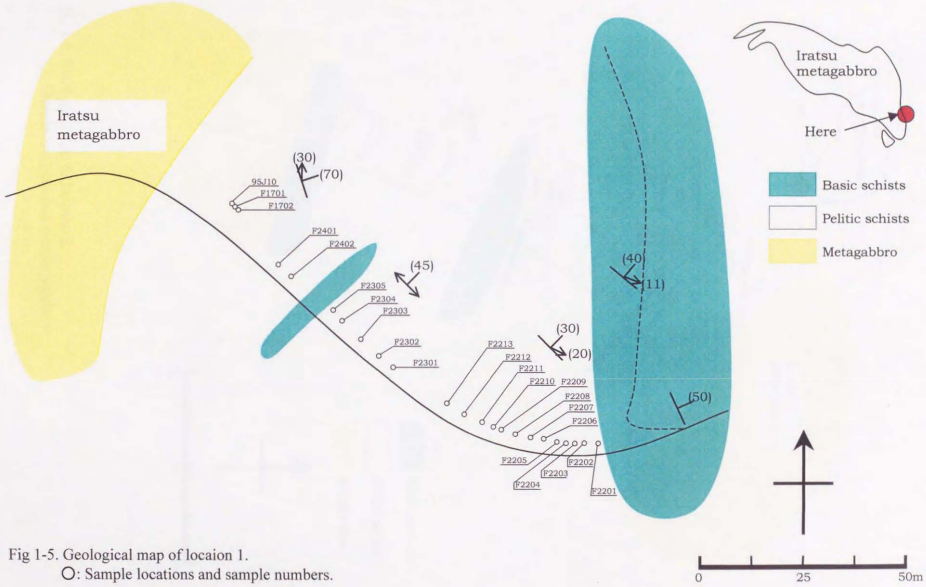

Fig 1-5. Geological map of locaion 1.
○: Sample locations and sample numbers.

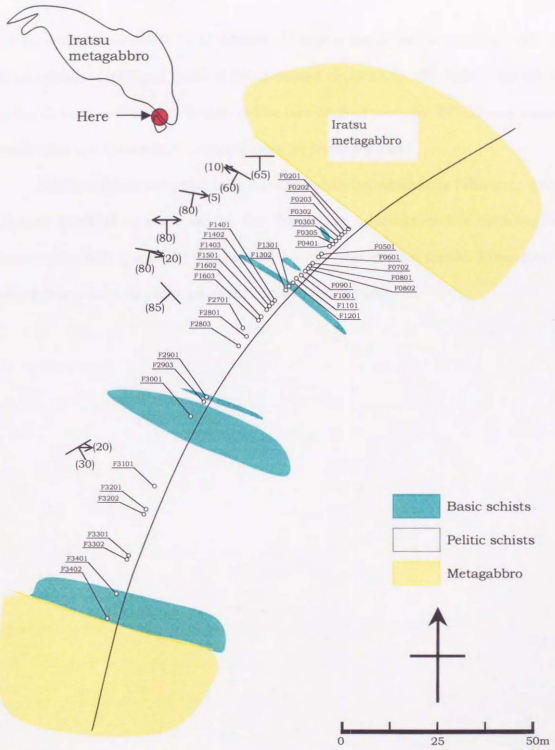

Fig 1-6. Geological map of location 2.
○: Sample locations and sample numbers.

thickness of around a few to 15 meters. Massive amphibolitic patches with the size as small as several tens of centimeters occured in the pelitic schists of location 1. They were identified near the locations of samples F0305 and F0902, though they are drawn in the map figure as basic schists.

Pelitic schists near the Iratsu mass exhibit conspicuous foliation, which is almost vertical in contrast to the dominant foliation of the Sambagawa metamorphic belt generally horizontal to 30° dip to the north. Lineation is nearly horizontal and sometimes difficult to determine.

2. Petrography

2-1. Indices for zonal classification

The Sambagawa metamorphic rocks of central Shikoku in the southwest Japan has been extensively investigated petrologically and geologically by many authors (e.g., Higashino, 1990a, b).

Several index minerals are used to define the metamorphic zones. The index minerals in the pelitic schists are garnet, biotite, and oligoclase. The appearance of the three minerals defines the lower boundary of the garnet zone, the albite-biotite zone, and the oligoclase-biotite zone, respectively. Appearance of hornblende is observed roughly at the same level as that of biotite. Typical mineral assemblages corresponding to each metamorphic zone are shown in figure 2-1. Pelitic schists in the chlorite zone are composed mainly of chlorite, albite, muscovite, and quartz.

The formation of garnet in the Sambagawa metamorphic belt can be written in a simple reaction:

$$\underset{\text{Chlorite}}{Mg_9Al_6Si_5O_{20}(OH)_{16}} + 4SiO_2 = 3\underset{\text{Garnet}}{Mg_3Al_2Si_3O_{12}} + 8H_2O$$
(Quartz)

Reactions regarding Fe and Mn end-members can be written in the same manner. Since it occurs earlier (lower grade) than the appearance of biotite, there is no other major minerals that contain abundant Fe and Mg. Other complex garnet forming reactions can be ignored. This reaction cannot be defined by univariant line, thus the formation of garnet is also controlled by bulk rock chemistry. It does not necessarily occur at the same temperature.

Several reactions can be written for the formation of biotite. Higashino (1975) proposed following reaction:

$$9K_2MgAl_3Si_7O_{20}(OH)_4 + Mg_9Al_6Si_5O_{20}(OH)_{16}$$
Celadonite Chlorite
$$= 3K_2Mg_6Al_2Si_6O_{20}(OH)_4 + 6K_2Al_6Si_6O_{20}(OH)_4 + 4SiO_2 + 8H_2O$$
Biotite Muscovite Quartz

It is not confirmed though, if biotite had been formed before the peak metamorphic condition keeping equilibrium with garnet (Higashino, 1975).

The formation of garnet or biotite is not strictly determined by univariant reactions. However, there is no large variation in the bulk rock chemistry found within the pelitic schists of the Sambagawa belt (Higashino, 1990). It is suggested by many previous studies that the appearances of those minerals approximately correspond to the same metamorphic grade. Therefore they are regarded as useful indices for zonal classification of pelitic schists in the Sambagawa metamorphic belt.

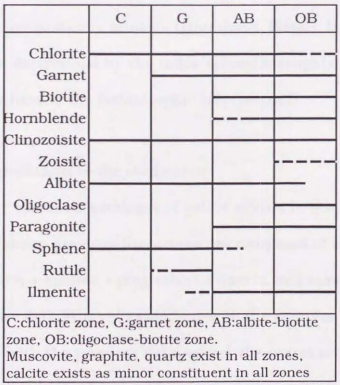

Fig.2-1. Typical mineral assemblages for pelitic schists in the Sambagawa metamorphic belt. Solid and broken line represents major and minor constituent, respectively. Modified from Enami (1983) and Takasu et al. (1994).

Oligoclase is usually identified at the rim portion of albite porphyroblasts in the oligoclase-biotite zone. It is considered to be the overgrowth formed under high temperature. Plagioclase solid solution is known to exhibit an unmixing composition range around An 2~5 % to An 20 %, which is called the peristerite gap. It is suggested that the gap closes at a temperature less than 600 °C, probably around 570 °C under the pressure condition of the Sambagawa metamorphic belt (Maruyama et al., 1982; Enami, 1981). Oligoclase appears only in rocks that are supposed to have reached the temperature of around 600 °C.

Distribution of the Fe and Mg between garnet and chlorite has been used as an indicator of temperature. It is shown that the $K_{Mg-Fe}^{Grt-Chl} \left(= (X_{Mg}^{Grt}/X_{Fe}^{Grt})/(X_{Mg}^{Chl}/X_{Fe}^{Chl})\right)$ values at the appearance level of particular index mineral approximately coincide (Higashino, 1990a). It suggests that the zone boundaries determined by the index minerals roughly correspond to isothermal contour lines of the metamorphic belt (isograd).

2-2. Mineral assemblages in the study area

Typical mineral assemblages of pelitic schists in the albite-biotite zone summarized by many previous literatures are composed of chlorite + garnet + biotite + muscovite + epidote + plagioclase + quartz, and sometimes hornblende and calcite (figure 2-1). Mineral assemblages in the samples used in this study largely coincide with the previous data, except the scarce occurrence of biotite. The representative mineral assemblage was garnet + muscovite + chlorite + plagioclase + quartz ± epidote ± hornblende, as shown in the figures 2-2,

2-3, and 2-4. Samples containing hornblende seemed to occur only in the vicinity of the tectonic blocks, although it may be accidental since the sampled locations are mainly near the tectonic blocks in the first place. Roughly about half of the samples contained epidote. Less than a third of the samples had biotite or hornblende.

Sphene and calcite are often present as accessory phases. Rutile is rarely found in the matrix of pelitic schists, but is often identified as inclusion minerals in garnet. Graphite is sometimes very abundant as inclusions in plagioclase porphyroblasts. Tourmaline and apatite is sporadically present.

It is remarkable that paragonite was almost ubiquitously identified as inclusion minerals in analyzed garnet grains from the albite-biotite zone. Paragonite is difficult to distinguish from muscovite with optical microscope, thus electron microprobe analysis was required. It is not described in the figure.

Micaceous minerals, mostly muscovite, are often clustered to form alternations of mica-rich and quartz-rich layers in pelitic rocks. Muscovite layers sometimes show kinked or buckled alignment that suggest intense deformation. Quartz in some samples shows fine grained, intertwined texture, which is suggestive of recrystallization during deformation. Tourmaline is the only mineral that shows obvious pull-aparts in the studied area.

Representative mineral assemblage of basic schists in the studied area is epidote + chlorite + hornblende + plagioclase + quartz $\pm$ garnet. Sphene is also present. Minor amount of talc rock is sometimes found at the boundary between mafic rocks and silicic pelites.

Observed mineral assemblage in the oligoclase-biotite zone was garnet + muscovite + chlorite + plagioclase + quartz $\pm$ hornblende $\pm$ epidote $\pm$

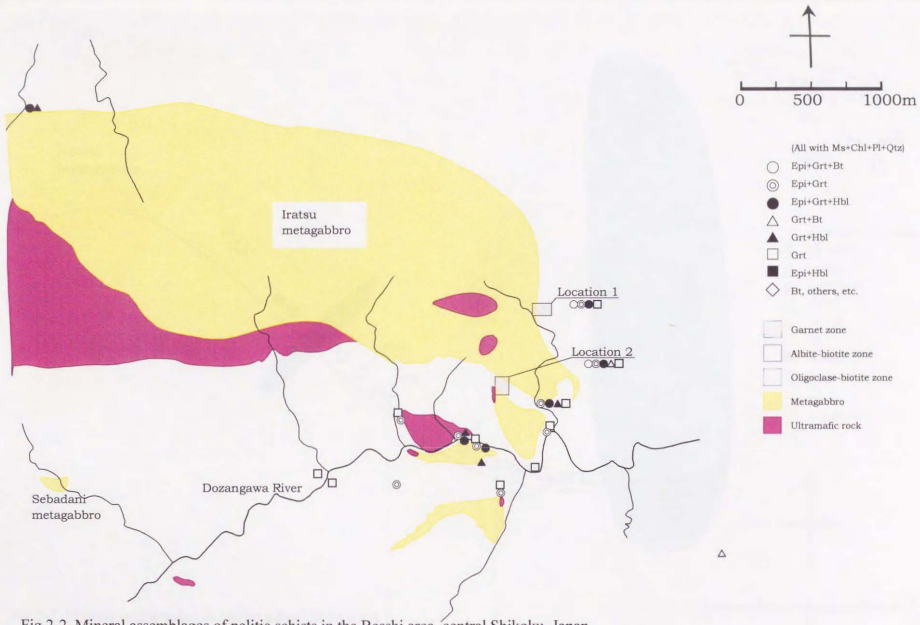

Fig.2-2. Mineral assemblages of pelitic schists in the Besshi area, central Shikoku, Japan.

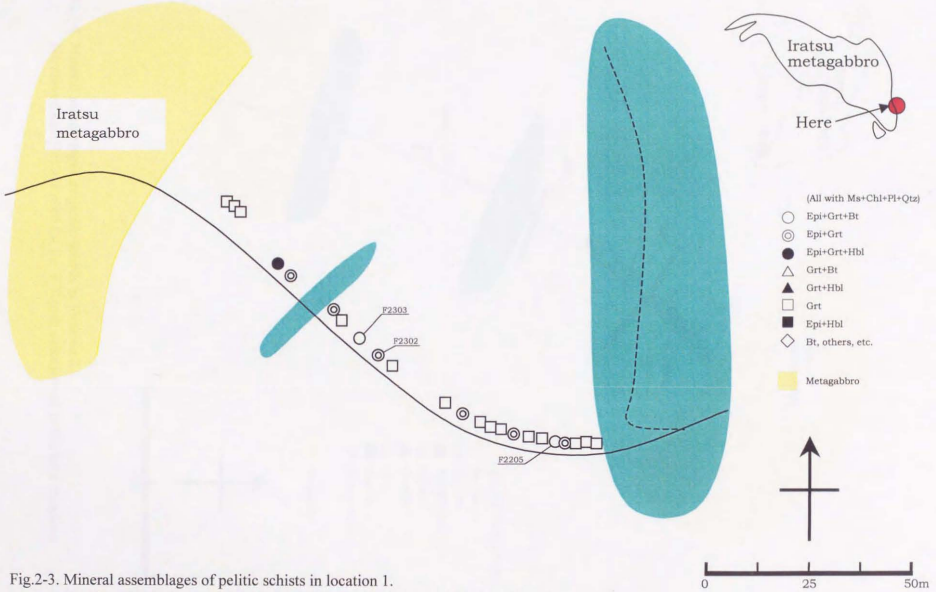

Fig.2-3. Mineral assemblages of pelitic schists in location 1.
Numbered samples are used for the P-T path calculations in the later chapters.

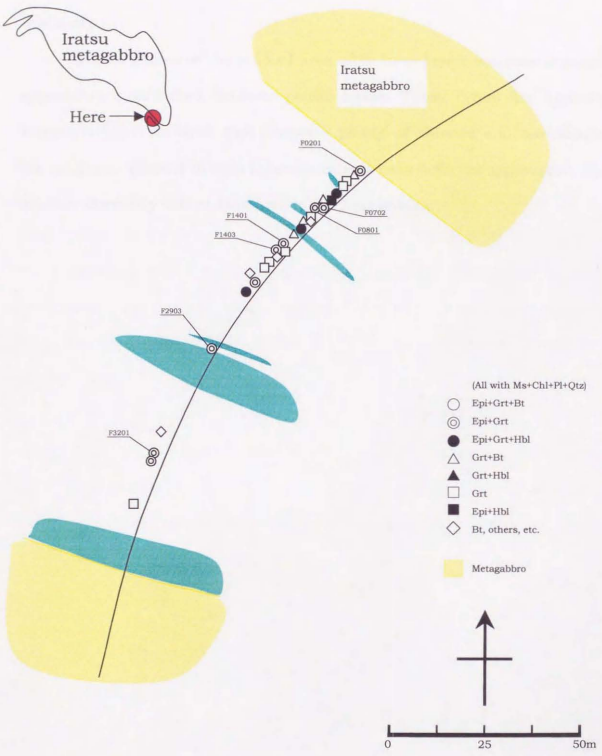

Fig.2-4. Mineral assemblages of pelitic schists in location 2.
Numbered samples are used for the P-T path calculations in the later chapters.

biotite. The existence of oligoclase was not confirmed by chemical analysis in this study.

Pelitic schists in the studied area often have layers with metabasaltic appearance sandwiched between pelitic layers. Those layers are typically several millimeters thick and comprise plenty of chlorite and hornblende. Garnet grains present in each layer sometimes have different appearance. The detailed chemistry will be examined in the next section.

3. Mineralogy

3-1. Garnet

3-1-1. Occurrence

Garnet occurs mainly as porphyroblastic grains in pelitic schists. The grain sizes of typical garnet in pelitic schists are 1 to 4 mm in diameter. Mica minerals forming the schistosity are often pushed aside by the garnet porphyroblast. Pressure shadows are well developed around garnet grains, which consist mainly of quartz. The shape of garnet is subhedral to rounded, indicating resorption after growth. There are also grains that have irregular but angular shapes due to cracking. Clustered chlorite is sometimes closely associated with garnet indicating that it grew consuming garnet during the retrograde stage.

Small garnet grains with diameter of 50 to 300μm are observed in some samples (fig.3-1). They often coexist with the typical garnet grains described above, which make the garnet population look apparently bimodal in size (fig.3-2). Most of the tiny garnet grains show clear and euhedral crystal surface,

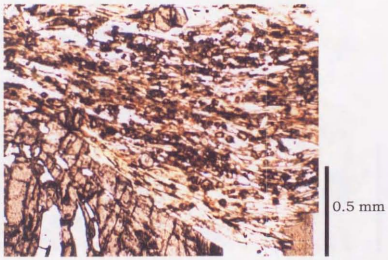

Fig.3-1. Photomicrograph of bimodal garnet grains (F3012). A normal large grain is in seen in the left below.

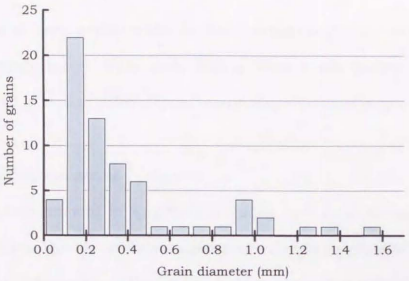

Fig.3-2. Bimodal grain size distribution of garnet (J2118). Diameters were measured in a thin section.

others are rounded as for the larger grains.

There are a few samples that clearly contain two distinct groups of garnet together (fig.3-3). One group is constituted with garnet grains with red tint and another with was pale pink garnet under optical microscope. Those samples often have layers with metabasaltic appearance sandwiched between pelitic layers. Those layers are typically several millimeters thick and comprise

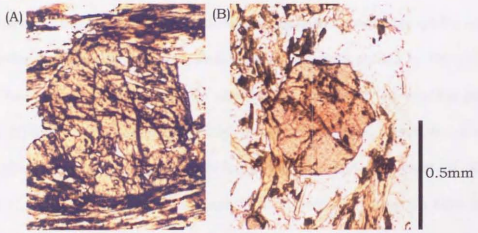

Fig.3-3. (A) A typical pelitic garnet grain and (B) a grain with red tint distributed around metabasaltic layers (F2803).

abundant chlorite and hornblende. Reddish garnet grains tend to locate in or around such layers. Pale pink grains with much quartz inclusions are distributed in typical pelitic layers comprising abundant muscovite and quartz.

3-1-2. Inclusion minerals

Large amount of quartz is included in typical garnet grains in the pelitic schists. Quartz crystals are commonly forming sigmoidal inclusion trails, indicating deformation of the host rock during garnet growth. Quartz inclusion trails are usually formed throughout the grains, not being truncated. Some of the garnet grains have quartz rich parts at the midst from the core to the rim, that look like quartz "rings". It is probably the cutting effect. Other minerals are also distributed overall within such grains. There are some samples in which inclusion minerals tend to occur near the core part of the garnet grain. Such grains do not exhibit clear sigmoidal inclusion trails. It is not yet clear how the difference is created in the distribution of inclusion minerals, since no clear difference is recognized in the configuration of quartz inclusions between the samples.

Minerals that are found as inclusions in garnet grains except for quartz are muscovite, paragonite, chlorite, and epidote. Epidote seems to be included nearer to the core of garnet. Rutile is also found mainly in the central part of the grain. Sphene is present but only in small amount. Previous studies described that rutile and sphene are found only in the core part of garnet (Banno et al. 1984), which is consistent with the observations in this study. Biotite and plagioclase is rarely found as inclusion minerals. Large amount of graphite is often included in garnet.

Garnet grains with red tint, that probably belong to metabasaltic layer, is poor in inclusion.

3-1-3. Normal zoning and composite zoning

Chemical zoning patterns of garnet were analyzed by an electron probe microanalyzer. Two dimensional mapping analyses were carried out. Their chemical composition trends from the core to the rim of representative grains were analyzed quantitatively.

Zoning patterns were classified basically into three categories: normal zoning, composite zoning, and sector zoning. Normal zoning is ubiquitously populated in the Sambagawa belt, where garnet is present. Mn content decreases from the core to the rim, forming so called "Bell shape" zoning. Mg, Fe, and Mg/Fe ratio increase from the core to the rim. These features are generally observed in garnet from relatively low temperature metamorphism, hence called "normal". It is believed to indicate increasing temperature during their growth. Observed Ca zoning, on the other hand, is not uniform within study area. With some samples, grossular concentration peaks at the midst between the core and the rim. Other samples contain garnet grains that show simple increase of CaO from the core to the rim. Thus, normal zoning can be further divided into two categories: Ca-rich normal zoning (fig.3-4), in which grossular content initially increases from the core and then start to decrease for the outer part, and Ca-poor normal zoning, which has Ca-poor core and grossular content keeps increasing toward the rim (fig.3-5). In the Sambagawa belt, Ca-poor type garnet has been reported only from the Oligoclase-biotite zone, Besshi district.

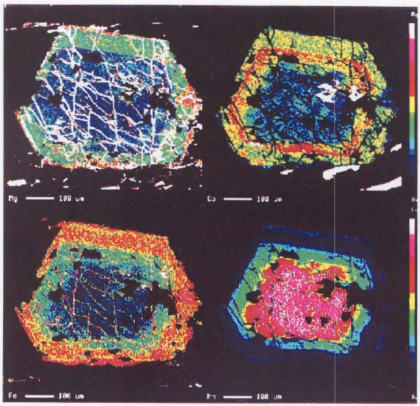

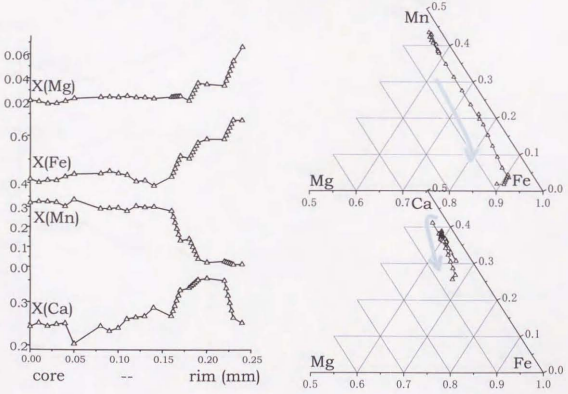

Fig.3-4. Chemical map analyses and chemical trends of Ca-rich normal zoning (F0702).

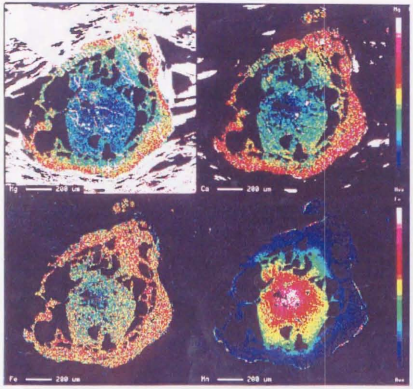

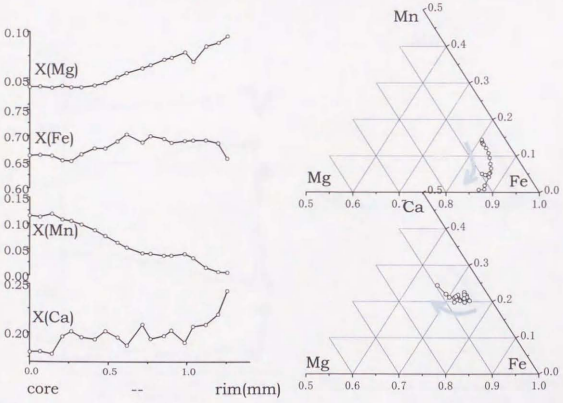

Fig.3-5. Chemical map analyses (F1401) and chemical composition trends (F1403) of Ca-poor normal zoning.

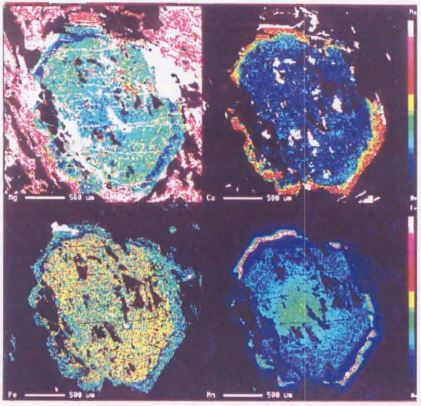

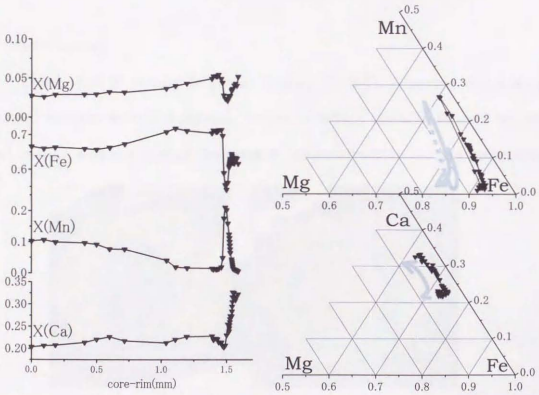

Fig.3-6. Chemical map analyses and chemical composition trends of composite zoning (F2903).

In garnet grains with composite zoning, spessartine content initially decrease from the core, shows an abrupt increase in the midst, and then start decreasing again as if forming normal zoning for a second time (fig.3-6). The shape of the crystal at the time of the sudden increase of Mn, being known from the chemical mapping image, is rounded to anhedral, in contrast with the mostly euhedral inner zoning. This suggests that these garnet grains were resorbed to some extent before they started growing again. Mg, and Fe also behave as if they formed normal zoning for two times with some time interval. Grossular content is low (15 to 20 mol%) during the inner portion and increases to as much as 35 mol% during the outer portion. The pattern is similar to the garnet zoning reported in the vicinity of the Sebadani metagabbro (Takasu, 1986; Nomizo, 1992).

3-1-4. Sector zoning

Third type of zoning is sector zoning (fig.3-7). A sector refers to a pyramidal domain within a crystal, border of which usually defined by one crystal surface and the core of the crystal. Material within certain sector had

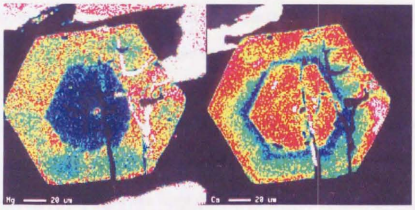

Fig.3-7. Chemical map analyses of sector zoning (F3101).
Note the difference of grain size between normal or composite grains and sector zoned grains.

been incorporated into the crystal through one particular crystal surface. The term "sector zoning" is normally applied to those cases when chemical composition is homogeneous in each sector, but differ from one sector to the other. Hourglass structure is a typical sector zoning. Sector zoning of garnet observed in this study, however, does not fit in this definition of sector zoning, since those grains show chemical heterogeneity within each sector. This type of zoning is called "intrasectoral zoning" in the strict sense (Paquette and Reeder, 1990). For simplicity, and also because there is no traditional sector zoning ever found in garnet, intrasectoral zoning in garnet will be called "sector zoning" throughout this paper.

Sector zoning is identified in chemical mapping images of all four end-members. Mg end-member tends to show heterogeneity more conspicuously than the other end-members, probably because the absolute concentration is low. It is observed that pyrope is more densely distributed at the central part of flat crystal surface, and other components (mainly observed in almandine and spessartine) are somewhat concentrated near the corner of the growing crystal. The pattern of chemical heterogeneity was sometimes rather vague and it was difficult to distinguish what element substituted what. However, the term "sector zoning" is applied whenever there is chemical heterogeneity not concordant with the growth surface of the grain.

A strong signature of microstructure in rocks containing sector zoned garnet is the obvious bimodal distribution of garnet grain size (fig.3-1). Typically, one group of garnet may consist of rounded grains of 1 to 2 mm in diameter, another of 0.1 to 0.3 mm and nearly euhedral. Tiny garnet grains are often concentrated in a quartz rich layer with a thickness of a few millimeters.

This texture usually indicates that the tiny ones have sector zoning. Nevertheless it is rare that "all" of the tiny grains exhibit sector zoning. Some of the samples with this textural signature even show no clear evidence for sector zoning.

Following criteria was adopted in this study, to designate the garnet grains in interest as sector zoning. (1) If some of the tiny garnet grains exhibited sector zoning, every grain that belongs to the group of tiny garnet will be identified as sector zoning. (2) If the group of tiny garnet grains had much different chemical composition compared to the other group, and also to each other within their own group, the tiny ones are designated as sector zoning, even if any of them are without observable intrasectoral heterogeneity.

3-1-5. State of coexistence of garnet grains with various zoning patterns

It is rather confusing that various patterns of chemical zoning are found mingled in such a small study area. To discover the history of the host rocks, it was essential to find out the history of garnet formation. Information was derived from the state of coexistence of various garnet grains within small hand specimens. Garnet grains in each hand specimen were classified into previous four zoning types: Ca-rich normal zoning, Ca-poor normal zoning, composite zoning, and sector zoning (Table 3-1 and 3-2). Chemical mapping analyses were made for more than one grain, around five, in each sample, to confirm every zoning type present in the particular sample will be detected.

A rule was discovered for coexistence of different zoning patterns: only garnet grains with sector zoning can coexist with another type of zoning in one hand specimen. Two, but no more, types of zoning can occur simultaneously in

Sample location	Sample No.	Ca-rich normal zoning	Ca-poor normal zoning	Compo-site zoning	Sector zoning	
(AB) In the vicinity of ultramafic rock	J2901		○		○	*
	J2902				○	
(AB) In the vicinity of metagabbro mass.	J3004		○		○	*
	J3005	○				*
	J3006	○				
	J3007	○				*
	J3010			○	○	
	J3011			○		
	J3101			○	○	
	J3102			○	○	* #
	J3105			○	○	
	J3107			○	○	
	J3109			○		
	J3110			○	○	#
	J3111				○	
	J3114		○		○	
	J3118		○		○	
	J2904			○		
	J2906	○				*
(OB) id.	J2013					
(AB) Ordinary Sambagawa schists.	J3012	○				
	J3013				○	
	J3015	○			○	

*: Minor growth at the outermost rim of normal or composite zoning.
#: Two groups of composite zoning in terms of chemical composition of the inner growth.

Table 3-1. State of coexistence between different zoning patterns of garnet in the study area. Samples in locations 1 and 2 are tabulated separately.

one sample, but in that case, one of them is always sector zoning and another is either normal or composite zoning. Composite zoning, Ca-poor normal zoning, and Ca-rich one never coexist with each other.

Detailed chemical analysis was applied to a few samples. Garnet grains were separated from the schists, to be cut right through the core. To take out individual garnet grains, the same heating and quenching procedure was adopted as Banno (1986). Garnet crystals were handpicked and embedded in resin. 1/4 to 1/3 of the diameter of the crystals was ground away, the surface polished, and analyzed preliminary. Backscattered electron image helped to

Sample locations	Sample No.	Ca-rich normal zoning	Ca-poor normal zoning	Compo-site zoning	Sector zoning	
(AB) Location 1 In the vicinity of the Iratsu metagabbro.	F2202				○	
	F2204	○			○	
	F2205	○				
	F2206	○			○	*
	F2208	○				
	F2210	○				
	F2211	○			○	*
	F2212	○				
	F2213	○				
	F2301	○				*
	F2302	○				
	F2303		○		○	*
	F2304	○				
	F2305	○			○	*
	F2401			○	○	*
	F1702			○		
	F1701			○		
	95J10			○		
(AB) Location 2 In the vicinity of the Iratsu metagabbro.	F0201		○			*
	F0202		○			*
	F0203		○			*
	F0302		○			
	F0303		○			
	F0305		○		○	
	F0401			○	○	
	F0601				○	
	F0702	○				
	F0801			○	○	
	F1001		○		○	*
	F1201	○				
	F1302		○			
	F1401		○		○	*
	F1402		○			*
	F1403		○			*
	F1602		○			*
	F1603		○			
	F2801			○		#
	F2803			○	○	* #
	F2901				○	B
	F2903			○		
	F3201			○		#
	F3302			○		
	F3401				○	B

*: Minor growth at the outermost rim of normal or composite zoning.
#: Two groups of composite zoning in terms of chemical composition of the inner growth.
B: Basic schist.

Table 3-2. State of coexistence between different zoning patterns of garnet in locations 1 and 2.

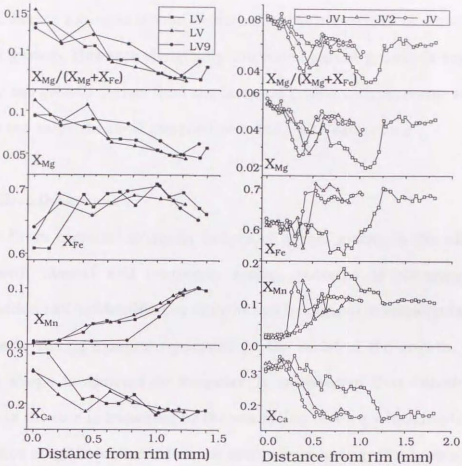

Fig.3-8. Comparisons of chemical trends from the precise core to the rim of grains within same samples. Left: Ca-poor normal zoning (96J3601 sector zoning occurs in this sample), right: Composite zoning (95J10).

locate the chemical core, before the grains were again cut perpendicular to the polished surface. This procedure assured the true chemical core to be exposed and analyzed. The result was that all "normal" or "composite" garnet grains contained in one sample recorded the same chemical composition trend throughout their growth from the core to the rim (fig.3-8). Hence it is suggested that chemical composition of garnet was controlled during most of their growth. Garnet most likely kept growing under near-equilibrium condition with other minerals in the matrix.

The same result was obtained from the sample having sector zoned

garnet. Sector zoning is a solid evidence for the occurrence of non-equilibrium crystal growth. However, chemically controlled garnet growth is suggested for most of the growth period, from the fact that grains without sector zoning have almost the same chemical composition trends with each other.

3-1-6. Growth textures

From chemical mapping images of garnet grains in the albite-biotite zone with normal and composite zoning, patterns of changing chemical composition can be identified as more or less hexagonal or rectangular in shape. Composite zoning exhibits resorption in the midst of the growth, where the crystal shape is rounded or irregular. It is observed that euhedral growth zoning in the core is truncated by the resorption texture, which implies that the resorption stage took place after the grains were once grown keeping euhedral shape (fig.3-9). Present shape of the garnet is also rounded or irregular to some extent, indicating resorption. Polygonal contour line is truncated by the current outline of the crystal.

The fact that the euhedral growth surfaces are still identifiable today suggests that the influence of diffusion was minor in those grains. Alteration of chemical composition due to diffusion should have erased the polygonal shape of the iso-chemical contours. The rate of cation diffusion in garnet is known to be generally low, that the influence is generally ignored for metamorphic rocks with peak temperatures lower than 600°C. The peak temperature for albite-biotite zone is around 520°C, as will be described in the next chapter. It seems reasonable to adopt the traditional view that no significant cation diffusion occurred in the study area.

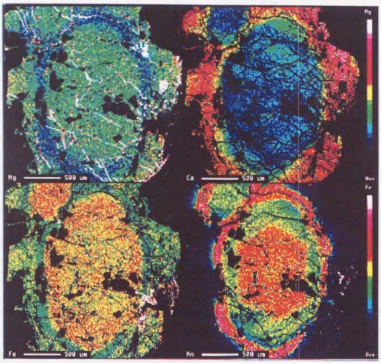

Fig.3-9. Chemical mapping analyses of garnet with composite zoning. Hexagonal growth surface is clearly observable as the iso-chemical contours inside the resorption texture.

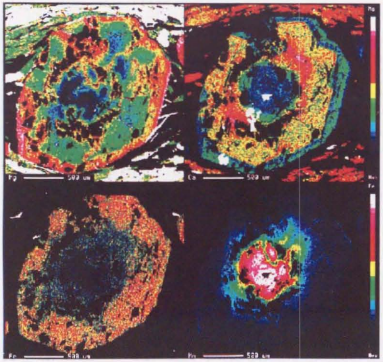

Fig.3-10. Chemical mapping analyses of garnet from the oligoclase-biotite zone (J2013). Chemical diffusion texture is obvious around inclusion minerals.

However in the oligoclase-biotite zone, garnet grains with evidences of cation diffusion are being found in this study (fig.3-10). It is observed that the polygonal growth texture is still obvious in the grain, especially in grossular. However, the chemical composition of the inner part of the crystal is altered. It seems that the part around included quartz is subject to intense cation diffusion, most likely turning into the same composition as the garnet rim (fig.3-11). It might suggest that the garnet grains were intruded by fluid phase, which was in equilibrium with the matrix, at the time of the growth of the garnet rim. The width of the diffusional texture (depth of the chemical alteration) is around 50μm. Although the alteration is small judging from the clear euhedral growth texture, it is seen that diffusion can drastically alter the chemical composition of garnet if there were large chemical gradient.

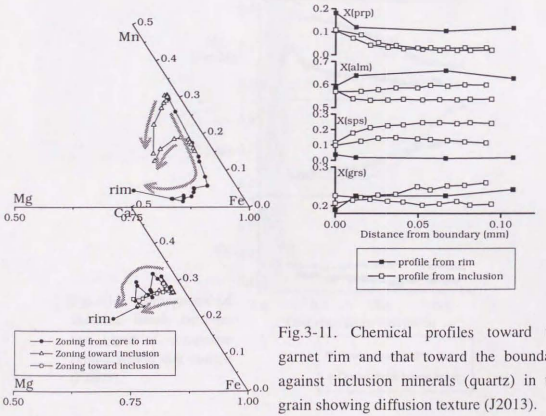

Fig.3-11. Chemical profiles toward the garnet rim and that toward the boundary against inclusion minerals (quartz) in the grain showing diffusion texture (J2013).

As described before, there were samples in which two types of garnet is present, one of them having deeper red tint. Neither of the two groups of garnet in such samples had sector zoning. Rather, both groups exhibited composite zoning (fig.3-12).

It is remarkable that chemical composition trend takes two distinct paths in the inner (first) normal zoning, converges after the resorption stage to form outer (second) normal zoning taking the same path (fig.3-13). Garnet grains from basaltic layer generally show chemical composition richer in Mg, compared to typical pelitic grains. However, this tendency only concerns to their inner part. When it comes to the outer part, namely the second prograde zoning, the composition converges with the second prograde zoning of pelitic grains.

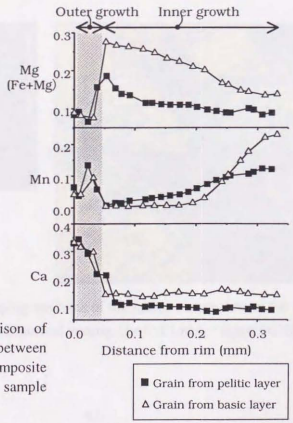

Fig.3-13. Comparison of chemical trends between two types of composite zoning within one sample (F2803).

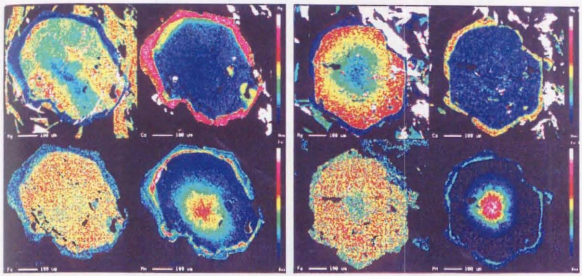

Fig.3-12. Chemical map analyses of garnet grains with two types of composite zoning from one sample. Left: grain from ordinary pelitic layer, right: grain from basaltic green layer. (F2803)

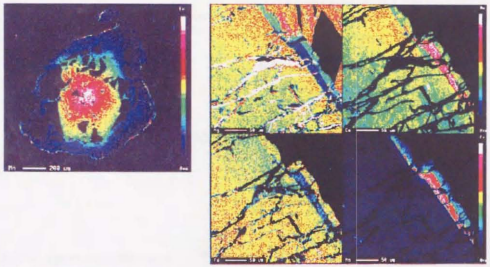

Fig.3-14. Chemical mapping analyses of the minor overgrowth at the rim of garnet grains with Ca-poor normal zoning. (Left: F1401; right: F0202).

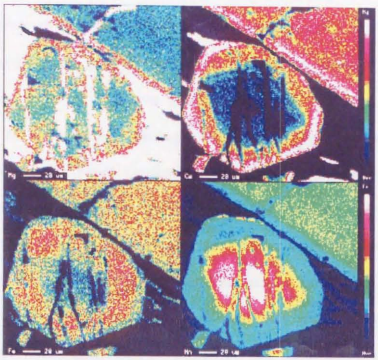

Fig.3-15. Chemical compositions coincide at the outermost rim of grains with normal zoning and sector zoning (F3102).

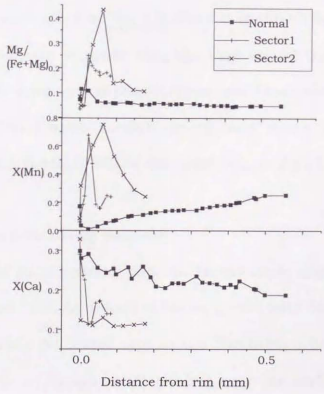

Fig.3-16. Chemical composition trend of garnet with normal zoning and the coexisting sector zoned garnet (F1401).

There are very thin (20～30μm in width) overgrowths at the very rim of the rounded garnet grains, where chemical composition shows abrupt change from normal pattern. The thin area is apparently rich in Mn, so that at first sight it seems to have formed through selective resorption of almandine or pyrope from the crystal. From detailed chemical analysis, however, it is found out that Mn content decreases again toward the true rim after the jump, demonstrating that the thin area represents another stage of growth (fig.3-14). This texture of thin overgrowth is found in grains with both normal and composite zoning. Thus normal zoning and composite zoning record twice and three times of growth stages, respectively.

Chemical mapping analysis with high spatial resolution has shown that the rim composition of the thin final growth and that of the coexisting sector zoning finally coincides with each other at the outermost 5 to 20μm (fig.3-15 and 3-16). This chemical agreement suggests that the very rim of the two groups of garnet formed simultaneously. It is possible to assume that most part of the normal or composite (=two times normal) zoning have grown under chemically controlled condition. This topic will be discussed later in detail.

3-1-7. Spatial distribution of various zoning patterns

Spatial distributions of garnet zoning patterns in the study area are shown in figures 3-17, 3-18, and 3-19. As described before, garnet with Ca-rich normal zoning is the most widely populated type in the Sambagawa belt. It occurs throughout the study area, though relatively less near the scattered tectonic blocks, including Iratsu metagabbro mass. Ca-poor normal zoning tends to occur near the tectonic blocks. Composite zoning occurs especially at

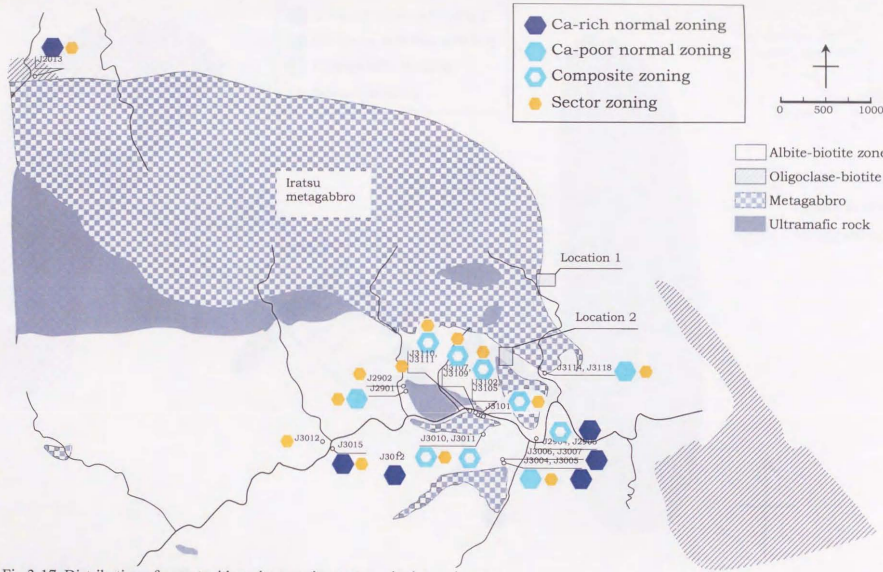

Fig.3-17. Distribution of garnet with various zoning patterns in the study area.
Location 1 and 2 are mapped separately in fine scale.

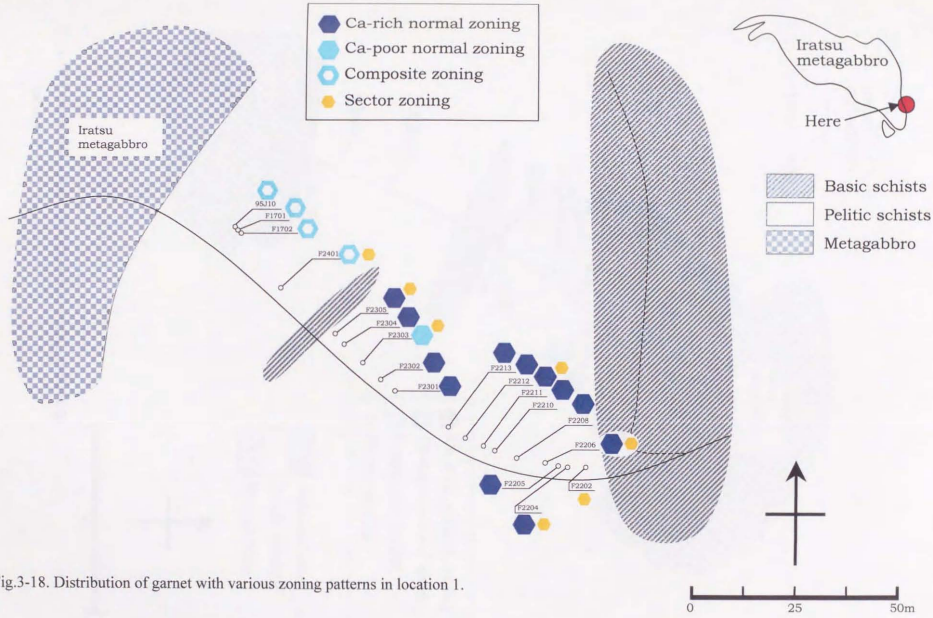

Fig.3-18. Distribution of garnet with various zoning patterns in location 1.

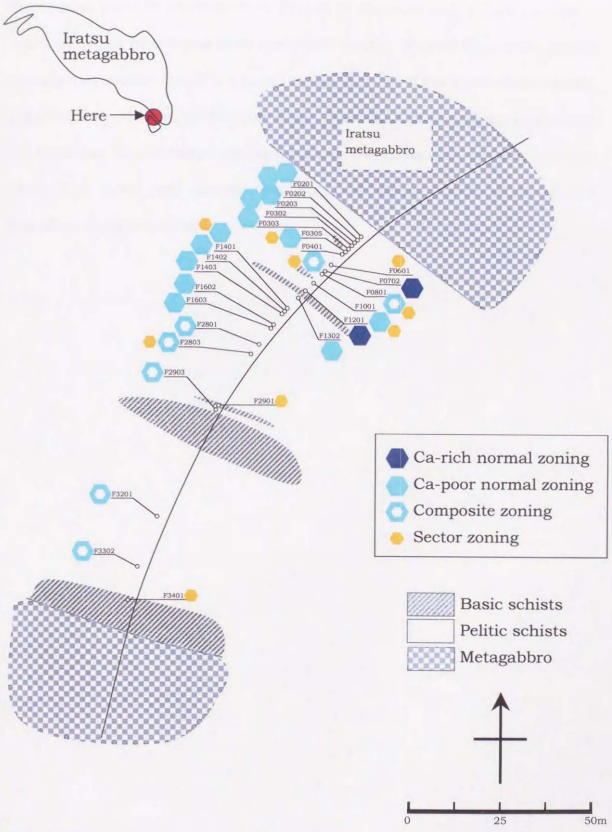

Fig.3-19. Distribution of garnet with various zoning patterns in location 2.

the nearest point to the boundary. Record of emplacement of tectonic blocks might be found in samples with composite zoning. Most of the garnet grains identified as sector zoning are found in the vicinity of the exotic rock masses, but some were at locations far from them. From the fact that sector zoning was not restricted to the boundary area against the exotic rock masses, it is not likely that those rock masses was the heat source which promoted the formation of sector zoning.

3-2. Muscovite

3-2-1. Occurrence

Muscovite is the dominant mineral defining schistosity in the pelitic schists. It composes up to 30 % of the volume of pelitic rocks by visual estimation. It often shows kinked alignment suggesting shear deformation. Anastomosing configuration of muscovite is found around large garnet porphyroblasts.

3-2-2. Chemistry

Chemical composition of muscovite is phengitic, which is known by pleochroism from pale purple to pale blue. Content of Mg and Fe cations per

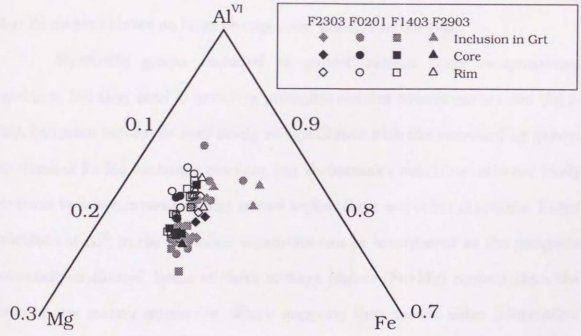

Fig.3-20. Chemical composition of muscovite. Solid symbols are the core composition of matrix muscovite, blank symbols are the rim composition, gray symbols are the composition of inclusion muscovite in garnet.

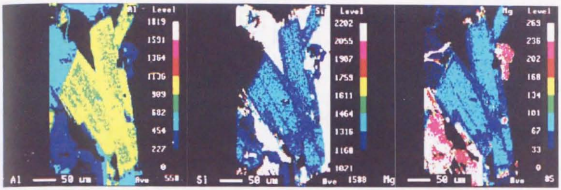

Fig.3-21. Chemical mapping analyses of muscovite in sample F2401.

formula unit ((Mg + Fe) / (Mg + Fe + Al^{VI})) is around 20 mol% or more in the core (fig.3-20). Highly phengitic composition of muscovite is common with other previous descriptions of biotite-free high-pressure metamorphic rocks from other regions in the world (Spear, 1993). Muscovite in the study area often has a rim with lower Mg content (around 10 %), which is clearly observable in the chemical mapping images (fig.3-21). Their rim shows higher Al^{VI} and lower Mg, but Fe content shows no large change from the core to the rim.

Muscovite grains included in garnet exhibit large compositional variance, but they tend to enrich in phengitic content toward garnet rim (fig.3-22). Inclusion muscovite may easily re-equilibrate with the surrounding garnet in terms of Fe-Mg exchange reaction, but Tschermak's substitusion is not likely to occur between muscovite and garnet unless there are other reactants. Large variance of Al^{VI} in the inclusion muscovite can be interpreted as the prograde composition change. Some of them contain higher (Fe+Mg) content than the core of the matrix muscovite, which suggests they record older information than the matrix.

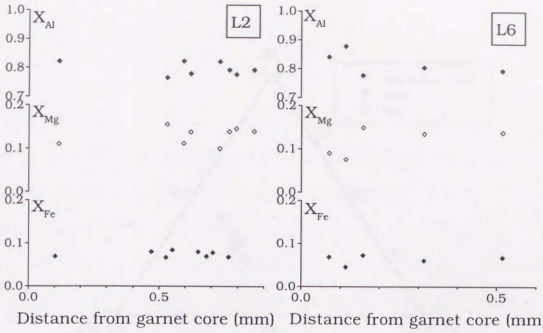

Fig.3-22. Chemical composition change of inclusion muscovite in garnet grains (F0201). Horizontal axis represents the location of the included muscovite in terms of the distance from garnet core.

3-3. Biotite

3-3-1. Occurrence

Biotite also helps forming foliation when it occurs abundantly. Such biotite shows clear crystal shape and cleavage obeying the schistosity, with deeper brown color under the microscope. On the contrary, some of biotite found in the study area are minor in amount and closely associated with chlorite. Tarnish texture of the latter type of biotite implies that they formed during retrograde reaction..

3-3-2. Chemistry

Higashino (1975) pointed out that biotite in the Sambagawa belt exhibited evidences of retrograde growth consuming garnet, and yet biotite

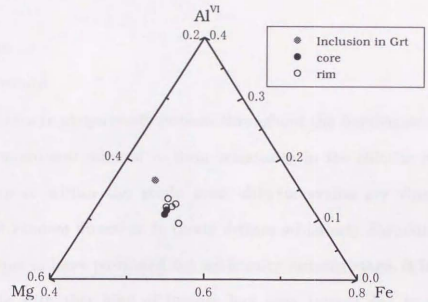

Fig.3-23. Chemical composition of biotite in sample F2205.

composition was nearly uniform in each sample. It suggests that the observed biotite no more keeps the equilibrium composition. On the other hand, Enami (1983) described different chemical composition of biotite defining the schistosity and that being formed within cracks of garnet. Mg-richer part of biotite that participate in the schistosity was thought to retain the prograde composition.

The X_{Mg} (= Mg / (Fe + Mg)) in analyzed biotite is 0.41 - 0.45, Al^{VI} is 0.1 – 0.13 (fig.3-23). These values plot at the poorer side of X_{Mg} and Al^{VI} of the previously reported average compositions (X_{Mg} = 0.47 $\pm$ 0.04, Al^{VI} around 0.13 (Enami, 1983)). Composition of retrograde biotite in the oligoclase-biotite zone deviates from prograde biotite in the same way (Enami, 1983). Though mineral composition depends on bulk chemical characteristics, it is not much likely that biotite in the area represents the composition at the time of prograde chemical

equilibrium.

3-4. Chlorite

3-4-1. Occurrence

Chlorite is ubiquitously present throughout the Sambagawa belt. It is the main constituent mineral to form schistosity in the chlorite and garnet zones. However within the study area, chlorite grains are clustered and arranged in random direction. It rarely defines schistosity. Formation of such chlorite seems to have postdated the schistosity forming stage. It is regarded that chlorite with this kind of texture has been formed due to retrograde reaction, most likely consuming garnet.

3-4-2. Chemistry

Composition of chlorite within each sample is homogeneous in most samples. X_{Mg} (Mg/(Mg+Fe)) is in the range of 0.4 to 0.6 (fig.3-24). However,

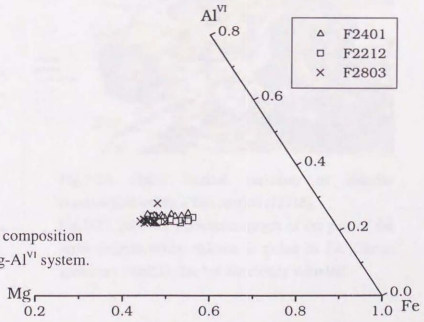

Fig.3-24. Chemical composition of chlorite in Fe-Mg-Al^{VI} system.

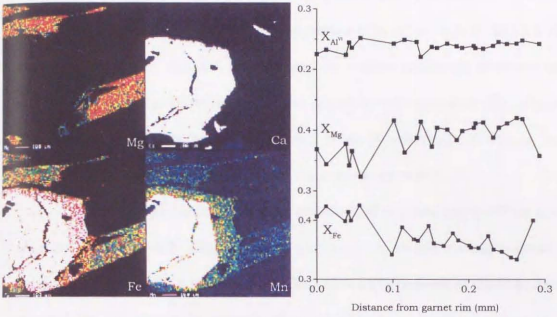

Fig.3-25. Chemical mapping analyses and composition trends of chlorite in direct contact with garnet rim. Part of chlorite in contact with garnet (found as a white grain on the left) is richer in Fe.

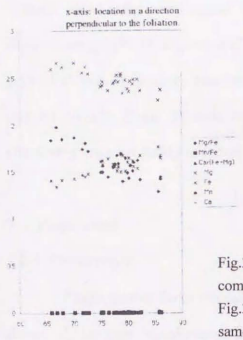

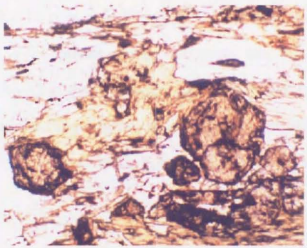

Fig.3-26. (left): Spatial variation of chlorite composition within a thin section (J2118).

Fig.3-27. (above): Photomicrograph of the part of the same sample where chlorite is richer in Fe. Garnet grains are small in size but are clearly euhedral.

where chlorite is in direct contact with garnet rim, composition of chlorite is apparently richer in Fe than the other parts of the same crystal (fig.3-25). If the chemical zoning of chlorite was formed by cation exchange reaction between garnet and chlorite, chlorite should get Mg-richer composition. The observation supports that chlorite was not altered through exchange reaction, but was formed through net transfer reaction consuming garnet.

Some samples exhibit spatial gradient of chlorite composition along the thin section (fig.3-26). Small garnet grains with sector zoning appear in the areas where chlorite is richer in Fe. The chemical gradient of chlorite cannot be created by the prograde growth of garnet, since chlorite enriches in Mg in response to the garnet growth. There are two possible interpretations for the observed chemical gradient of chlorite: (1) Fe-richer chlorite was formed by the retrograde reaction consuming garnet, (2) Garnet with sector zoning was formed selectively consuming the Fe-rich matrix chlorite. It is seen in the photomicrograph of figure 3-27, that garnet grains maintain the euhedral crystal shape. It is more reasonable that garnet grains with sector zoning was formed locally from Fe-rich chlorite. The initial inhomogeneity of chlorite chemistry was probably created by chlorite forming reaction consuming garnet.

3-5. Plagioclase

3-5-1. Occurrence

Plagioclases form conspicuous spots with diameter of 1 to 5 mm. The shape of the spot is anhedral. They often include large amount of graphite, as well as many other minerals such as quartz, epidote, and garnet. It does not have any trace of pressure shadow. Plagioclase spot is thought to have formed

in the later stage of metamorphism, judging from the chemical zoning of included garnet (Sakai et al., 1985).

3-5-2. Chemistry

Plagioclase composition is almost pure albite, with ~2 % anorthite. No oligoclase is observed in the analyzed samples, consistent with the metamorphic grade. Some samples exhibit plagioclase with Ca-rich core (fig.3-28 and 3-29). Part of plagioclase rim in other samples is slightly richer in anorthite. The shape of chemical zoning of Ca in the latter case is not clearly concentric, but is rather patchy. It is not yet confirmed whether it is growth zoning or not.

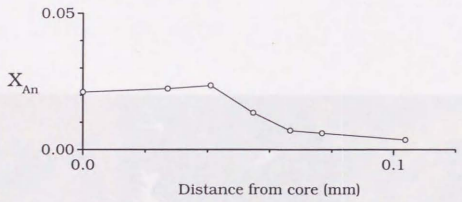

Fig.3-28. Chemical composition trend from the core to the rim of plagioclase (F2903).

3-6. Epidote

3-6-1. Occurrence

Epidote is found in about half of the samples of pelitic schists. Epidote crystals have prismatic shape, largely forming the schistosity. They are

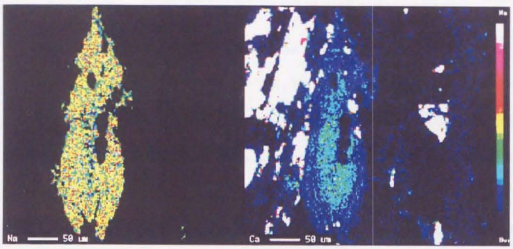

Fig.3-29. Chemical mapping analyses of plagioclase in sample F2401.

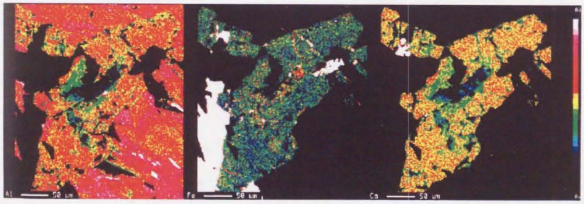

Fig.3-30. Chemical mapping analyses of clinozoisite in sample F1403. Al decreases at the outermost rim. The allanitic core is recognized as the Ca poor part in the core.

colorless and exhibit low birefringence under optical microscope. Some of the grains have brownish core.

3-6-2. Chemistry

Chemical composition of epidote in the matrix is Al-rich, with X_{Fe}^{3+} (= Fe^{3+} / (Al + Fe^{3+})) of around 15 %. No zoisite is identifiable based on chemical composition. Epidote is chemically zoned with the core richer in Fe^{3+} end-member (pistacite), and it generally decreases from the core toward the rim (fig.3-30 and 3-31). Pistacite then starts to increase again near the rim. The brownish core recognized under optical microscope has allanitic composition, with Ce and other light rare earth elements concentrated to as much as over 10 wt%.

Inclusion epidote within garnet exhibits higher Al content that

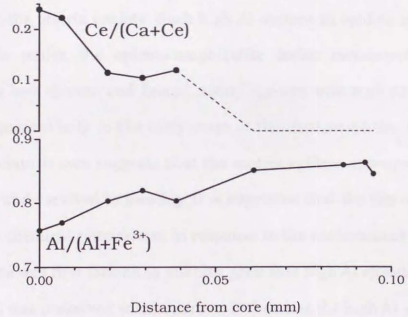

Fig.3-31. Chemical zoning of epidote from the allanitic core to the rim (F2903). Ce concentration is calculated assuming all the missing mass can be ascribed to Ce.

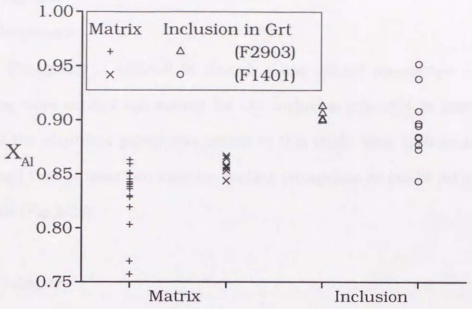

Fig.3-32. Comparison of chemical composition of epidote in the matrix and that included in garnet. $X_{Al}=X_{Al}/(X_{Al}+X_{Fe^{3+}})$. Sample F2903 and F1401 contain garnet with composite zoning and that with Ca-poor normal zoning, respectively.

approaches 90 % in terms of Al / (Al + Fe^{3+}). The same composition range is not observed in the matrix epidote. Such high Al content in epidote is supposed to be unstable under the epidote-amphibolite facies metamorphism of the Sambagawa belt (Enami and Banno, 1980). Epidote with high Al content may have been present only in the early stage of the metamorphism. On the other hand, the allanitic core suggests that the matrix epidote appeared in the very early stage and survived to this day. It is suggested that the rim of epidote has changed its chemical composition in response to the environment from time to time. Epidote was first formed as allanite, grew into high Al epidote in the early stage which was preserved within garnet. It then lost the high Al portion in the rim to exhibit the zoning currently observed.

3-7. Paragonite

3-7-1 Occurrence

Paragonite is difficult to identify using optical microscope. Chemical analyses were carried out mainly for the inclusion minerals in garnet, thus most of the identified paragonite grains in this study were inclusions. It was confirmed that at least two samples contain paragonite as one of major matrix minerals (Fig.3-33).

3-7-2 Chemistry

Paragonite is the only phase that contains Na as a major component except for albite. All analyzed paragonite grains were almost pure phase. Paragonite is usually treated as an end-member composing muscovite-paragonite solid solution. In the study area, paragonite exists as an individual phase with 1 to 3 mol% of muscovite (K / (Ca + K)).

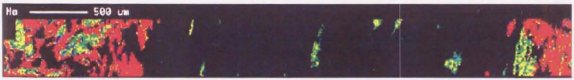

Fig.3-33. Chemical mapping analysis of Na in the matrix showing the presence of paragonite (seen as green-yellow) together with plagioclase (red) (F1403).

4. Previous studies of pressure-temperature conditions

4-1. The Sambagawa metamorphism

Peak metamorphic conditions of each metamorphic grade of the Sambagawa belt have been deduced using several geothermobarometries, and the results are briefly summarized by Enami et al. (1994) (fig.4-1). Estimated peak temperatures for the garnet zone and the albite-biotite zone are 440± 15 °C and 520 ± 25 °C , respectively, applying the garnet-chlorite geothermometer (Grambling, 1990) and garnet activity model from Hodges and Spear (1982). The highest temperature condition for the oligoclase-biotite zone rocks is 610±25°C according to Enami (1983), determined from garnet-biotite geothermometry calibrated by Pigage and Greenwood (1982). Metamorphic pressure had been more or less obscure because of the chemical characteristics of the Sambagawa schists, which commonly contain plagioclase with very low anorthite content. Using Na-pyroxene in quartz schists, Enami et al. (1994) estimated the peak pressure to be 5.5 – 6.5 kbar at the chlorite zone, 7 – 8.5

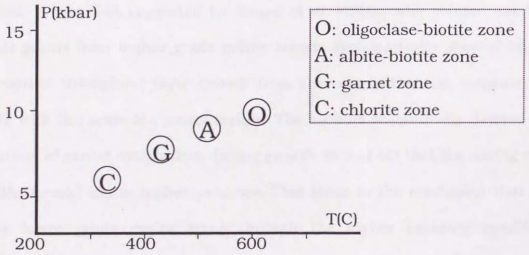

Fig.4-1. Previous estimation of the peak P-T condition for the Sambagawa metamorphic belt. The circle approximates to the error range. (Modified after Enami et al. (1994)).

kbar at the garnet zone, 8 – 9.5 kbar at the albite–biotite zone of Asemigawa area. For the oligoclase-biotite zone, 9.3 – 10.6 kbar is the deduced pressure applying garnet-biotite-muscovite-plagioclase geobarometer (Ghent and Stout, 1981). Enami (1983) utilized a reaction, 4zoisite + quartz = 5anorthite + grossular + $2H_2O$, to confirm the estimation. Overall field P-T gradient is 1.4 – 1.8 kbar/100 °C (Enami et al., 1994).

Enami et al. (1994) noted that the peak pressure and temperature conditions are not uniform within each metamorphic grade. Quartz schists from Sarutagawa area in the north systematically gave higher pressures compared to those at the same temperature from Asemigawa and Besshi area described above. This configuration is interpreted to be an evidence of north-dipping isotherm at the time of metamorphism.

P-T paths for individual rocks have come to the fore in accordance with progresses in chemical analysis technique. From chemical zoning in minerals such as garnet and amphibole, different paths for each metamorphic grade are implied. It was first suggested by Banno et al. (1986), who pointed out that garnet grains from higher grade pelitic schists systematically showed higher Mg content throughout their growth from the core to the rim, compared at points with the same Mn concentration. The authors theoretically derived the transition of garnet composition during growth, to find out that the zoning with low Mg formed under higher pressure. This leads to the conclusion that the whole lower grade region went through the higher pressure condition. Amphibole zoning may also support this view. Amphiboles from high grade schists apparently lack the core of glaucophanic amphibole, which is present in the amphiboles from low grade (Hara et al., 1990; Enami 1994). It can be

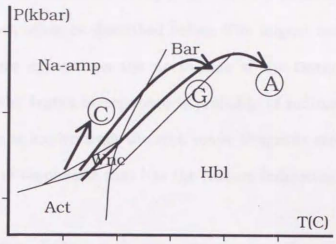

Fig.4-2. Supposed P-T history for each metamorphic grade zone deduced from chemical zoning of amphiboles. (Modified after Enami, 1994(J))

explained by assuming lower pressure paths for the higher temperature zones (fig.4-2).

A great number of studies have postulated that a heating process continued into the early exhumation stage. One of the major arguments is based on the fact that the grossular content in garnet peaks in the midst of garnet growth from the core to the rim (Enami, 1998). Grossular content is widely regarded as an indicator of pressure. This type of chemical zoning behavior is observed extensively in the Sambagawa belt. There are still other evidences indicating decompression at the latest stage, though it is not clear whether the decompression belongs to the prograde event or not. This topic will be discussed later in detail.

4-2. Tectonic blocks

Tectonic blocks having ultramafic and metagabbroic origin are exposed

as lenticular rock masses in the study area. The rock masses show different P-T histories to each other, as described before. The largest tectonic block is the Iratsu metagabbro exposed on the north side of the Dozangawa River. The western part of the Iratsu metagabbro is probably of sedimentary origin, and prograde eclogite is known from the rock mass. Prograde eclogite is identified by the existence of omphasite that has the texture indicating prograde growth (Takasu, 1984).

The eastern Iratsu rock mass is metamorphosed layered gabbro. Transitional features from the granulite facies or the hornblende eclogite into the amphibolite facies are occasionally found (Takasu, 1984; Kunugiza et al., 1986). This observation tells the history of the eastern Iratsu mass as follows: firstly it formed under 10 kbar pressure as a layered gabbro, secondly metamorphosed in the granulite facies, followed by eclogite facies, and then incorporated into the Sambagawa belt during the epidote-amphibolite facies stage.

Detailed analysis based on chemical compositions of garnet and omphacite suggests that the eastern Iratsu mass experienced two distinct stages of the eclogite facies metamorphism: (1) high temperature eclogite facies (700 - 800°C, 15 - 20 kbar) and (2) low temperature eclogite facies (600-700°C, 10 - 15 kbar). A stage of temperature increase from the epidote-amphibolite facies toward the low temperature eclogite facies is recognized between the two eclogite stages (Toriumi and Kohsaka, 1994). Considering that the east and west Iratsu rock masses are finally reequilibrated under epidote-amphibolite facies metamorphism, the P-T history of the tectonic blocks is depicted as figure 4-3.

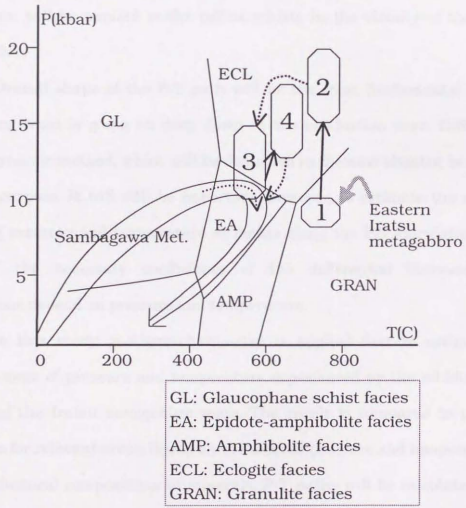

Fig.4-3. Previous estimation of the P-T history of the Sambagawa metamorphic belt and the Eastern Iratsu metagabbro mass. Numbers 1～4 represent the time sequence. (modified after Kunugiza et al. (1986), Takasu (1989), Wallis and Banno (1990), Toriumi and Kohsaka (1995)).

5. Geothermobarometry

Focus of this study is to deduce the history of pressure and temperature change experienced by the rocks to discover the evidence for the emplacement of the tectonic blocks. Geothermobarometry and differential thermodynamic calculation will be applied to the pelitic schists in the vicinity of the Iratsu metagabbro.

Overall shape of the P-T path will be the most fundamental clue for unraveling what is going on deep down in the subduction zone. Differential thermodynamic method, which will be described in the next chapter, is suitable for this purpose. It will still be important, however, to estimate the absolute values of pressure and temperature at points along the P-T calculation, since most of the necessary coefficients of the differential thermodynamic calculations depend on pressure and temperature.

In this study, geothermobarometry is applied first to estimate the general range of pressure and temperature experienced by the schists in the vicinity of the Iratsu metagabbro mass. The result is compared to previous estimates for relevant areas. Based on the derived pressure and temperature as well as chemical compositions of minerals, P-T paths will be calculated using differential thermodynamic method in the next chapter.

Absolute pressure-temperature estimation is a common practice in studies of metamorphic rocks, and many geothermo- and geobarometers have been proposed for pelites.

As for the higher grade metapelites of the Sambagawa belt, the biotite isograd locates at the higher temperature side than the garnet isograd. The coverage of garnet-biotite Fe-Mg exchange geothermometer is limited, though it

is one of the most extensively applied calibrations in the world. Instead, the garnet-chlorite Fe-Mg exchange geothermometry (Grambling, 1990) has generally been used in this region (Enami et al., 1994).

It is known that care must be given to which composition to choose for use in the garnet-chlorite geothermometry. Two types of chlorite have been described in the Sambagawa metamorphic belt. One type has clear shape and defines the mineral lineation of the rock, another is aggregated crystals that extend to random direction. Only former type of chlorite is suitable for use in temperature estimation, since the latter type is presumably produced through retrograde reaction consuming garnet (Higashino, 1975). In the study area, however, such lineation-defining chlorite is rarely found, to make the application of the garnet-chlorite geothermometer inadequate. Thus some other indicators had to be adopted in this study.

The garnet-biotite Fe-Mg exchange geothermometry is applied to biotite-bearing samples. It has been pointed out that most of the observed biotite may not maintain the composition at the time in equilibrium with garnet (Higashino, 1975). Therefore the derived temperature is tentative, but will be useful to compare the result with previous estimations. As an alternative means, the garnet-phengite Fe-Mg exchange geothermometry (Hyndman and Forest, 1988) is applied in order to estimate whether there are temperature differences between biotite-bearing and biotite-free samples.

Reactions between Ca end-members of garnet and plagioclase contribute to pressure estimation. Numerous geobarometers are proposed that involve various other minerals such as aluminosilicates, Ti minerals, and mica minerals. However, accuracy of the garnet-plagioclase geobarometry is doubtful

in this area since anorthite concentration is very low (Todd, 1998). For instance, application of GRIPS geobarometer (Bohlen and Liotta, 1986) demonstrates that an error of 0.5 % in anorthite concentration leads to a variance of nearly 1 kbar of calculated pressure. Moreover, activity-composition relationship of anorthite is not yet experimentally constrained for this lowest composition range. Fairly large value is expected for activity coefficient of anorthite, error in which significantly affects the calculation as well as the composition. Since range of anorthite content is unsuitable, some other indicators are required for pressure estimation. Major Ca-bearing phase in studied schists except for grossular and anorthite is epidote. Clinozoisite content in epidote is tested to make a geobarometer in this study using available thermodynamic data.

5-1. Garnet-biotite geothermometer

Among a number of proposed geothermometers, the most popular is the calibration of the Fe-Mg exchange reaction between garnet and biotite (Thompson, 1976; Ferry and Spear, 1978; Hodges and Spear, 1982; Pigage and Greenwood, 1982; Perchuk and Lavrent'yeva, 1983; Bhattacharya et al., 1992; Holdaway et al., 1997; Gessmann et al., 1997). It uses the following exchange reaction as the indicator:

$$KMg_3AlSi_3O_{10}(OH)_2 + Fe_3Al_2Si_3O_{12} = KFe_3AlSi_3O_{10}(OH)_2 + Mg_3Al_2Si_3O_{12}$$

Phlogopite Almandine Annite Pyrope

On applying garnet-biotite geothermometry, the first and the most critical step is to choose which model to use. There is considerable discrepancy between many of the proposed calibrations. Utilization of one particular

calibration sometimes leads to a result more than 100 °C different from that of another. Enami (1983) applied three garnet-biotite geothermometers to the oligoclase-biotite zone schists. Temperature derived using the calibration by Pigage and Greenwood (1982) was higher than those derived from Thompson (1976) and Ferry and Spear (1978) by 100 °C or more. Enami (1983) pronounced the former value to be more reliable, for the latter two classic experiments used Mn- and Ca-free garnet, their nonideal behaviors not being considered. It is but difficult to judge whether this view is correct, because widely dispersed calibrations are still being proposed in recent years. For instance, formulation by Holdaway et al. (1997) produces lower temperatures close to that derived by Ferry and Spear (1978). In contrast, that by Gessmann et al. (1997) produces temperatures on the higher side.

Calibration by Gessmann et al. (1997) is applied in this study for two reasons: it is one of the latest published calibrations, and it extracts consistent temperatures compared to the formerly adopted garnet-biotite thermometry to the Sambagawa metamorphic belt. The purpose here is to test whether the recorded temperatures in the studied schists agree with previous data for relevant areas. The ground does not seem to be firm yet to propose a totally original geothermometric result. It is more important to keep consistency with geothermometries previously applied.

Experimental data of Gessmann et al. (1997) was obtained in the temperature range 600 - 800 °C at the pressure of 2 kbar, using synthetic phases as starting materials. Biotite is considered as a three component system involving Tschermak's substitution, namely Fe-Mg-Al system, in contrast to the traditional simplification that treated biotite as strictly binary Fe-Mg system.

All Fe in biotite is considered as ferrous iron. On application, quaternary garnet activity model by Ganguly et al. (1996) was inserted into the binary expression of Gessmann et al. (1997).

The results for the two biotite bearing samples were 547 °C and 484 °C (fig.5-1) at 9 kbars (previous pressure estimation from Enami et al. (1994)). Both were calculated using average compositions of each mineral in the sample: composition at the rim of garnet, and Mg-richer core composition of biotite. The garnet rim of sample F2303 showing the thin overgrowth with irregular chemical composition was not used. The result for sample F2205 is in agreement with the estimated temperature of 520 °C ± 25 °C for the albite-biotite zone. There are two possible reasons for the temperature deviation of sample F2303. Garnet grains in sample F2303 exhibit resorption texture in considerable amount, and also the thin overgrowth at the final stage is observed. Chemical composition of garnet at the time of equilibrium is difficult to estimate. Another observation is that biotite inclusion is not found within the garnet grains of sample F2303. If biotite appeared after the termination of

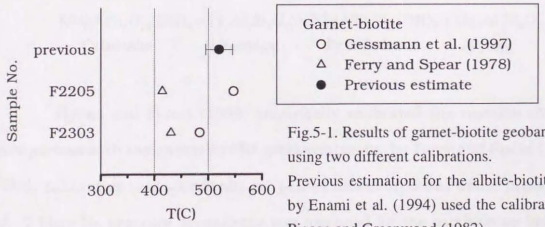

Fig.5-1. Results of garnet-biotite geobarometry using two different calibrations. Previous estimation for the albite-biotite zone by Enami et al. (1994) used the calibration by Pigage and Greenwood (1982).

garnet growth, it means that the garnet and biotite with observed compositions have never been in equilibrium. It is suggested that the result from sample F2205 is more reliable.

The model of Gessmann et al. (1997) always produced higher temperatures than that of Ferry and Spear (1978). Temperatures derived by the model of Ferry and Spear (1978) is 431°C and 415°C for samples F2205 and F2303, respectively (fig.5-1). The differences between the derived temperatures of the two calibrations under the probable pressure of 9 kbar was 55 - 130°C, which was strongly dependent on the Al^{VI} content of biotite. The higher the Al^{VI} content, the lower the difference.

5-2. Garnet-phengite geothermometer

Biotite-free metamorphic rocks are rather common in high pressure metamorphic terranes. It is known that muscovite in those rocks is often phengitic, containing much Fe and Mg. The garnet-phengite Fe-Mg exchange reaction has been calibrated as an alternative temperature indicator for the garnet-biotite geothermometry (Hynes and Forest, 1988). The exchange reaction utilized is as follows:

$$\underset{\text{Celadonite}}{KMgAlSi_4O_{10}(OH)_2} + \underset{\text{Almandine}}{Fe_3Al_2Si_3O_{12}} = \underset{\text{Fe-celadonite}}{KFeAlSi_4O_{10}(OH)_2} + \underset{\text{Pyrope}}{Mg_3Al_2Si_3O_{12}}$$

Hynes and Forest (1988) empirically calibrated the reaction through comparison with the garnet-biotite geothermometer by Ferry and Spear (1978). Their calibration was specifically for pelites metamorphosed under pressure of 3 - 7 kbar. No pressure dependence was assumed for the partitioning between

garnet and muscovite. Krogh and Raheim (1978) and Green and Hellman (1982) also calibrated the Fe-Mg exchange reaction between garnet and phengite using high pressure experiments at 25 - 30 kbar. They proposed geothermometers for >10 kbars through empirical calibration using natural samples. Previous estimation of pressure for the albite-biotite zone is 8 - 9.5 kbar. Calibration by Hynes and Forest (1988) is adopted in this study, for the pressure range is more suitable.

The results for the biotite-bearing samples were 426°C and 410°C (fig.5-2). Both results were derived using average compositions of each mineral. Chemical compositions of the Mg richer core of muscovite and the rim of garnet were used. Again, the thin and irregular overgrowth at the outermost rim of

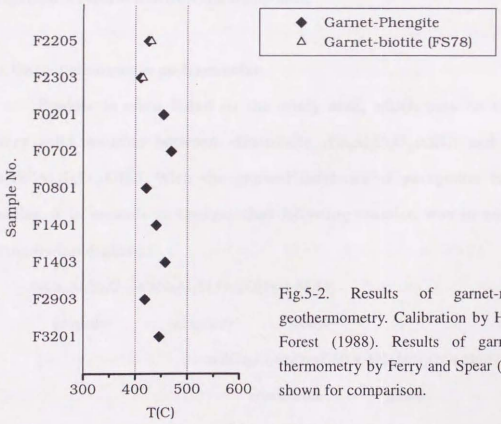

Fig.5-2. Results of garnet-muscovite geothermometry. Calibration by Hynes and Forest (1988). Results of garnet-biotite thermometry by Ferry and Spear (1978) are shown for comparison.

garnet was avoided. Muscovite is present in large amount, and thus the final overgrowth may have little influence on the core composition of muscovite. Systematic deviation is inherent in the calibration of Hynes and Forest (1988), since it is calibrated to the garnet-biotite geothermometer by Ferry and Spear (1978), which derives significantly lower temperature as described in previous section. From comparison, it is obvious that the garnet-phengite calibration matches the temperature derived by Ferry and Spear (1978) with errors of around 5 °C.

Results for other studied samples are in the range of 400 - 470 °C. In spite of the large uncertainty expected from the empirical calibration, as well as of the scarcity of sample number, it is quite well in accordance with each other. It can be said that at least there is no large variance of peak temperature recorded within the study area.

5-3. Garnet-clinozoisite geobarometer

Epidote is often found in the study area, which may be treated as binary solid solution between clinozoisite ($Ca_2Al_3Si_3O_{12}(OH)$) and pistacite ($Ca_2Fe^{3+}Al_2Si_3O_{12}(OH)$). With the general existence of paragonite in studied samples, it is possible to assume that following reaction was in equilibrium during metamorphism:

$$4Ca_3Al_2Si_3O_{12} + 5NaAl_3Si_3O_{10}(OH)_2 + 6SiO_2$$

grossular paragonite quartz

$$= 6Ca_2Al_3Si_3O_{12}(OH) + 5NaAlSi_3O_8 + 2H_2O$$

clinozoisite albite

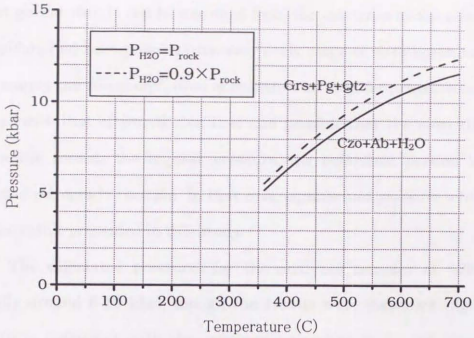

Fig.5-3. Univariant curves of the garnet-clinozoisite reaction applied to sample F2205.

This reaction involving clinozoisite and grossular has a univariant curve with low dP/dT that can potentially serve as a geobarometer (fig.5-3). Thermodynamic properties such as molar enthalpy, entropy, and volume of each phase were taken from Holland and Powell (1998). Mixing property of garnet was taken from Ganguly et al. (1996). Fe^{3+} in epidote was treated that it preferably occupies one particular site among the three Al sites. P_{H2O} is assumed to be equal to environmental pressure (P_{rock}). This assumption does not introduce large error. If P_{H2O} was 90 % of environmental pressure, calculated pressure will be less than 1 kbar higher (at 500°C) than the presented result below.

Epidote usually shows chemical zoning as described before. Clinozoisite content is poor in the core, increases outward, then decreases at the outermost rim. It is difficult to estimate which composition was in equilibrium with the

present garnet rim. It can be assumed from the existence of the allanitic core that epidote had been present from very early stage of metamorphism. In this study, simply the rim composition of epidote was used for pressure estimation, together with that of garnet rim. It is still possible that the most clinozoisite rich mantle records the highest pressure, the outermost portion being the product of retrograde reaction. In that case, equilibrium pressure will be lower than the result presented in this study.

The calculated pressures for the analyzed samples at 520°C were generally around 8-10 kbar, though the results were dispersed (fig.5-4). The pressure is consistent with the previous estimation of 8 - 9.5 kbar for the albite-biotite zone (Enami et al., 1994).

Together with the results from geothermometers, it is confirmed that there is no large anomaly in the final state of the temperature-pressure condition in the study area. The schists record average temperature and

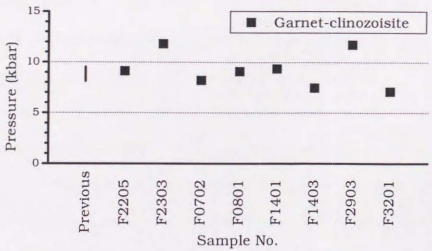

Fig.5-4. Calculated pressure for the study area using the garnet-clinozoisite reaction curve. Previous estimation for the albite-biotite zone from Enami et al. (1994).

pressure concordant with the surrounding albite-biotite zone, even though they contain anomalously zoned garnet grains such as composite zoning and sector zoning. The event that caused those anomalous growths must have occurred during metamorphic recrystallization, long before the peak condition currently observable in the matrix minerals was achieved.

6. Differential thermodynamic method

Differential thermodynamic method has been developed specifically to calculate relative changes of intensive variables based on changes of chemical conditions. It is a suitable means to calculate the pressure-temperature history from the chemical zoning of minerals. Garnet provides the required information about the change of chemical environment from one particular moment to the next.

Based on the derived pressure and temperature range as well as the chemical compositions of minerals, P-T paths experienced by each garnet grain can be calculated. Different paths deduced from different zoning patterns of garnet should contain crucial information concerning the emplacement of the tectonic blocks.

6-1. Method

Differential thermodynamic method was originally established by Spear and Selverstone (1983), and has been applied to many cases successfully (Selverstone et al., 1984; Kohn et al., 1992). Japanese readers can refer to Ikeda (1995) for detailed explanation of the method.

Metamorphic rocks are heterogeneous systems that comprise many phases (minerals) consisting of many system components (SiO_2, Al_2O_3, etc.). Assuming the whole system is in equilibrium, chemical equilibrium for each system component can be formulated. Consequently the whole system is described with a set of simultaneous equations. The basic procedure of the differential thermodynamic method is to solve the thermodynamic equations for the equilibrium of metamorphic rocks. The major problem is that those

simultaneous equations are highly non-linear. Taylor's series expansion will convert non-linear equations into linear equations, which for the first time are ready to be solved by simple algorithm. Those linear equations relate "differences" of the variables involved. Chemical zoning in garnet is an excellent monitor for change of mineral compositions along the time axis. Using chemical composition changes in garnet as monitor parameters, it is possible to derive pressure and temperature change.

6-2. Formulation

In multi-phase systems like metamorphic rocks, each system component must be in equilibrium with other coexisting phases as well as within each phase. That is, chemical potential, μ, of each system component is supposed to be the same in all phases within the system. One equation can be written for each system component:

$$\mu^{A}_{SiO_2} = \mu^{B}_{SiO_2} = \mu^{C}_{SiO_2} \cdots$$

where A, B, ... represent minerals. Chemical potential, namely molar Gibbs free energy, of each system component is not directly observable. Differential thermodynamic method therefore introduces mineral end-member compositions to the formulation. Firstly, thermodynamic equilibrium is written in terms of stoichiometric relations between chemical potentials of mineral end-members:

$$\sum_{i=1}^{n} \nu_i \mu_i = 0 \qquad (6\text{-}1)$$

where i represents mineral end-members, ν_i is stoichiometric coefficient for the relation. This equation expresses that chemical potential change due to the

described reaction is equal to zero. Chemical potential is then related to chemical composition through the activity term:

$$\mu_i = \mu^\circ_i + RT\ln(a_i) \qquad (6\text{-}2)$$

μ°_i is the chemical potential of pure phase at the temperature and pressure of interest, which is generally a function of P and T. a_i is the activity term, which plays the role of introducing the thermodynamically nonideal behavior of minerals into the equations. $a_i = a_i(X_i)$ or $a_i = a_i(P,T,X_i)$.

When all the phases involved are pure, the second term of the equation (6-2) can be ignored ($a_i = 1$). Substituting $\mu_i = \mu^\circ_i$ into the equation (6-1) and a little modification makes the following equation:

$$0 = \sum \nu_i \mu^\circ_i = \Delta G_R = \Delta H_R - T\Delta S_R$$

$$= \Delta H^\circ_R + \int_{298}^{T} C_p dT - T(\Delta S^\circ_R + \int_{298}^{T} \frac{C_p}{T} dT) + \int_{1}^{P} \Delta V_R dP \qquad (6\text{-}3)$$

Subscript "R" represents "reaction", that is, ΔH_R is the change of enthalpy due to the specific reaction. C_p also represents the change of heat capacity due to the reaction, though the subscript "R" is not written for simplicity. Available data of mineral thermodynamic property is generally at the standard state of 25°C and 1 bar for pure phases. The actual formulation needs to be calibrated for temperature and pressure as written in (6-3). ΔH°_R and ΔS°_R represent enthalpy and entropy of reaction at the standard state.

Solid solution phases are often present in rock systems, where $a_i \neq 1$. When the second term of equation (6-2) is substituted into equation (6-1), an additional term appears to make the total equation as follows:

$$\Delta G_R = 0 = \Delta H^\circ_R + \int_{298}^{T} C_p dT - T(\Delta S^\circ_R + \int_{298}^{T} \frac{C_p}{T} dT) + \int_{1}^{P} \Delta V_R dP + RT \ln K \qquad (6\text{-}4)$$

$$K = \prod a_i^{\nu_i} \qquad (6\text{-}5)$$

K is the equilibrium constant.

Here, pressure and temperature are formulated into an equation expressed with activities of mineral end-members, which are then related to compositions. This is the basic equation that represents thermodynamic constraint.

Number of independent constraints is uniquely determined for each system, and is equal to the number of independent reactions. It is obtained as follows:

(number of independent reactions)
= (number of phase components) – (number of system components).

"Phase components" is the mineral end-members.

Every system has certain number of degree of freedom according to Gibbs phase rule:

(degree of freedom) = (number of system components) + 2 – (number of phases)

Degree of freedom represents the difference between the number of independent variables and that of thermodynamic constraints. Independent variables are temperature, pressure, and molar fraction of each mineral end-member. If degree of freedom is zero, there are the same number of variables and equations, which means every variable must have fixed value. If degree of freedom is more than one, there are more independent variables than the number of constraints. Equations can be solved for unknown variables only

when part of the variables are given somehow. If sufficient number of mineral compositions are known, one can solve the simultaneous equations for pressure, temperature, and other unknown mineral compositions. The required number is equal to the degree of freedom.

Equation (6-4) is nonlinear. It is not realistic to solve several of such equations simultaneously. A simple procedure to linearize the equation is to apply Taylor's series expansion. If higher order terms are ignored, Taylor's series expansion is, for instance, as follows:

$$\Delta G_R(T,P,\cdots)=0 \qquad (6\text{-}6)$$
$$=\Delta G_R(T_o,P_o,\cdots)+\left.\frac{\partial \Delta G_R(T,P,\cdots)}{\partial T}\right|_{T=T_o,P=P_o,\cdots}(T-T_o)+\left.\frac{\partial \Delta G_R(T,P,\cdots)}{\partial P}\right|_{T=T_o,P=P_o,\cdots}(P-P_o)+\cdots$$

None of the partial derivatives in the equation (6-4) by P, T, and X_i will contain the enthalpy term, ΔH°_R, since it is constant. Enthalpy term is eliminated from the equation through this treatment, thus the possible error due to the uncertainty in enthalpy data can be avoided. This is a significant merit of this transformation. It is possible to solve the overall system now that the thermodynamic constraints are written with linear equations.

As for mineral compositions, number of independent variables is ((number of end-member) – 1) for each solid solution. It is more practical to include all end-members into formulation. To do this, one needs to set stoichiometric constraints in addition to the thermodynamic equilibrium constraints in the form of (6-6). This constraint simply expresses that the sum of end-member contents for each mineral must be equal to 1:

$$\sum_i X_i = 1$$

It should be noted that differential thermodynamic method always

treats "relative" values, as is clear from (6-6). Stoichiometric constraints are actually incorporated as follows:

$$\sum_{i} \Delta X_i = 0 \qquad (6\text{-}7)$$

Altogether, two groups of equations can be written for heterogeneous systems of metamorphic rocks: thermodynamic constraints (6-6) and stoichiometric constraints (6-7). Number of the stoichiometric constraints is equal to the number of solid solutions, and also to the number of additional variables. The number of equations increases, but the matter is the same from mathematical point of view.

Required known values, according to the degree of freedom of the system, must also be given as differences. Garnet zoning provides the required value of compositional change from one time to another. The quaternary solid solution of garnet supplies three independent variables. If the degree of freedom of a system is equal to or less than three, chemical composition of garnet is enough to solve the equations for all other variables including temperature and pressure. By solving the equations step by step from the core composition of the mineral toward the rim, history of temperature and pressure change during garnet growth is calculated successively. If absolute temperature and pressure is known for one or more point along the path, the whole history of intensive variables can be unraveled.

6-3. System

Chemical composition of garnet is the prime factor used to decipher the time series of metamorphic conditions. It is essential to know which mineral

was in equilibrium with garnet during its growth. Mineral assemblage at the time of garnet growth was estimated from inclusion minerals in garnet as well as current mineral assemblage in the matrix.

As described before, typical mineral assemblage in the study area is garnet + chlorite + muscovite + plagioclase + quartz. Clinozoisite, biotite, hornblende, and other accessory minerals occur in some samples. Paragonite is not identified in all samples, since it is recognized only by chemical analysis, but is confirmed as matrix mineral in some of the analyzed samples.

Inclusion minerals in garnet grains give strong evidences to speculate the coexistent matrix minerals in the past. Quartz, muscovite, paragonite, chlorite are almost ubiquitously identified as inclusion minerals. Epidote is often present in garnet grains in the samples that contain epidote in the matrix. Biotite and plagioclase inclusions are scarce in amount. Plagioclase can be assumed to have been present throughout prograde metamorphism, based on many previous observations. On the other hand, biotite is not supposed to have been present during garnet growth, unless it is found as inclusion minerals in garnet.

Samples with mineral assemblage garnet + chlorite + muscovite + paragonite + clinozoisite + plagioclase + quartz + water $\pm$ biotite was chosen and modeled in this study. The end-members used in the calculation is tabulated in table 6-1. Required system components are Fe_2O_3-MnO-Na_2O-CaO-K_2O-FeO-MgO-Al_2O_3-SiO-H_2O. Degree of freedom for this system is 3 (biotite-bearing system) or 4 (biotite-free system). Ten samples were quantified for the calculation, which contained the above mineral assemblage both as inclusion and matrix minerals. One exception is paragonite, which was

Mineral	End-member	Formula unit
Garnet (Grt)	Pyrope (Prp)	$Mg_3Al_2Si_3O_{12}$
	Almandine (Alm)	$Fe_3Al_2Si_3O_{12}$
	Spessartine (Sps)	$Mn_3Al_2Si_3O_{12}$
	Grossular (Grs)	$Ca_3Al_2Si_3O_{12}$
Biotite (Bt)	Phlogopite (Phl)	$KMg_3AlSi_3O_{10}(OH)_2$
	Eastonite (Eas)	$KMg_2Al_3Si_2O_{10}(OH)_2$
	Annite (Ann)	$KFe_3AlSi_3O_{10}(OH)_2$
	Mn-biotite (Mnb)	$KMn_3AlSi_3O_{10}(OH)_2$
Muscovite (Ms)	Muscovite (Ms)	$KAl_3Si_3O_{10}(OH)_2$
	Celadonite (Cel)	$KMgAlSi_4O_{10}(OH)_2$
	Fe-celadonite (Fec)	$KFeAlSi_4O_{10}(OH)_2$
Paragonite (Pg)		$NaAl_3Si_3O_{10}(OH)_2$
Chlorite (Chl)	Clinochlore (Cch)	$Mg_5Al_2Si_3O_{10}(OH)_8$
	Amesite (Ame)	$Mg_4Al_4Si_2O_{10}(OH)_8$
	Daphnite (Dap)	$Fe_5Al_2Si_3O_{10}(OH)_8$
	Mn-chlorite (Mnc)	$Mn_5Al_2Si_3O_{10}(OH)_8$
Epidote (Epi)	Clinozoisite (Czo)	$Ca_2Al_3Si_3O_{12}(OH)$
	Pistacite (Ptc)	$Ca_2Fe^{3+}Al_2Si_3O_{12}(OH)$
Plagioclase (Pl)	Albite (Ab)	$NaAlSi_3O_8$
	Anorthite (An)	$CaAl_2Si_2O_8$
Quartz (Qtz)		SiO_2
Water		H_2O

Table 6-1. Mineral end-members used in the differential thermodynamic calculations.

assumed to have been present even if it is not found in the matrix, since it is not identified optically. One of the samples contained biotite as inclusion mineral. Biotite was assumed to have stayed in equilibrium with garnet, after the first appearance of the inclusion biotite. Ti minerals were not involved in the model, since their stability is not ascertained. Fluid phase was assumed to be pure H_2O, and no CO_2 was considered.

6-4. Thermodynamic data and mixing properties of minerals

Thermodynamic data such as entropy, molar volume, and heat capacity for each mineral end-member were taken from the internally consistent data set of Holland and Powell (1998) (table 6-2). Activity-composition relationships were constructed using the latest studies as shown in table 6-3. Detailed descriptions of the activity models in table 6-3 are given below. Data set of Holland and Powell (1998) required the use of specific activity models for most of the minerals, since the data were dependent on the activity models.

6-4-1. Garnet

Garnet is generally treated as quaternary solid solution between pyrope, almandine, spessartine, and grossular. Fe^{3+} content is very small in studied garnet and is ignored. Mixing occurs on three equivalent sites in a formula unit, thus ideal part of the activity of each end-member is written as $a_{prp} = X_{prp}^3$, etc. Substantial non-ideality has been known in the thermodynamic behavior of garnet. Fortunately, garnet has kept attracting workers' attention for a long time, so that there are abundant data available for the mixing property of

ij	W_{ij}^H(J/mol)	W_{ij}^S(J/K·mol)	W_{ij}^V(J/bar)
MgFe	2117	0	0.07
FeMg	695	0	0
MgMn	12083	7.67	0.04
MnMg	12083	7.67	0.03
MgCa	9834	5.78	0.058
CaMg	21627	5.78	0.012
FeMn	539	0	0.04
MnFe	539	0	0.01
FeCa	6773	1.69	0.03
CaFe	873	1.69	0
MnCa	6773	1.69	0.03
CaMn	873	1.69	0

Table 6-4 Margules parameters for the asymmetric solid solution model of garnet proposed by Ganguly et al. (1996). $W_{ij}^G = W_{ij}^H - TW_{ij}^S + (P-1)W_{ij}^V$.

	$\Delta_f H$ (J)	S(J/K)	V(J/bar)	a(J/K)	b(J/K^2)	c(JK)	d(J/$\sqrt{K}$)
Pyrope	-6284230	266.3	11.318	633.5	0	-5196100	-4315.2
Almandine	-5263650	340	11.511	677.3	0	-3772700	-5044
Spessartine	-5646300	367	11.792	584.6	-0.001593	-7516700	-2750.1
Grossular	-6644070	255	12.535	626	0	-5779200	-4002.9
Phlogopite	-6219440	328	14.964	770.3	-0.036939	-2328900	-6531.6
Eastonite	-6348940	306	14.751	785.5	-0.038031	-2130300	-6893.7
Annite	-5143440	428	15.432	825.7	-0.034861	19800	-7466.7
Mn-biotite	-5463500	433	15.264	809.9	-0.059213	-1514400	-6998.7
Muscovite	-5984120	292	14.083	756.4	-0.01984	-2170000	-6979.2
Celadonite	-5844480	287	14.04	741.2	-0.018748	-2368800	-6616.9
Fe-celadonite	-5497320	318	14.25	756.3	-0.019147	-1586100	-6928.7
Paragonite	-5946330	276	13.211	803	-0.03158	217000	-8151
Clinochlore	-8929860	410.5	21.09	1161.8	0.010133	-7657300	-9690.9
Amesite	-9052530	390	20.52	1177	0.009041	-7458700	-10053
Daphnite	-7153990	545	21.34	1237.4	0.013594	-3743000	-11250
Mn-chlorite	-7680490	580	22.59	1227.8	-0.02699	-6299800	-10469.4
Clinozoisite	-6898110	301	13.63	567	0.018063	-7034000	-2603
Pistacite	-6463200	328	13.91	544.6	0.02478	-11230000	-1192.1
Albite	-3934600	210.1	10.006	452	-0.013364	-1275900	-3953.6
Anorthite	-4233480	200	10.079	371.6	0.012615	-4110200	-2038.4
Quartz	-910880	41.5	2.269	110.7	-0.005189	0	-1128.3
Water	-241810	188.8	2.2	40.1	0.008656	487500	-251.2

$\Delta_f H$: enthalpy of formation from the elements, S : entropy, V : volume, C_p = heat capacity = $a + bT + cT^{-2} + dT^{-1/2}$

Table 6-2. Molar thermodynamic properties of mineral end-members used in the differential thermodynamic calculations in this study. Data are from Holland and Powell (1998).

End-member	Mole fraction (Xi)	Activity (ideal part)	Activity (nonideal part)
Pyrope	$X_{Mg} / (X_{Mg} + X_{Fe} + X_{Mn} + X_{Ca})$	$(X_{prp})^3$	Asymmetric regular solution model from Ganguly et al. (1996)
Almandine	$X_{Mg} / (X_{Mg} + X_{Fe} + X_{Mn} + X_{Ca})$	$(X_{alm})^3$	
Spessartine	$X_{Mg} / (X_{Mg} + X_{Fe} + X_{Mn} + X_{Ca})$	$(X_{spt})^3$	
Grossular	$X_{Mg} / (X_{Mg} + X_{Fe} + X_{Mn} + X_{Ca})$	$(X_{grs})^3$	
Phlogopite	$1 - X_{eas} - X_{ann} - X_{Mnb}$	$(X_{eas} + X_{phl})^2 X_{phl} (1 + X_{eas})(1 - X_{eas})$	Symmetric regular solution model, W from Holland and Powell (web)
Eastonite	X_{Al}^{VI}	$\frac{1}{4}(X_{eas} + X_{phl})^2 X_{eas} (1 + X_{eas})^2$	
Annite	$\left(X_{Fe} / (X_{Mg} + X_{Fe} + X_{Mn})\right)\left((3 - X_{ms})/3\right)$	$X_{ann}^3 (1 + X_{eas})(1 - X_{eas})$	
Mn-biotite	$\left(X_{Mn} / (X_{Mg} + X_{Fe} + X_{Mn})\right)\left((3 - X_{ms})/3\right)$	$X_{Mnb}^3 (1 + X_{eas})(1 - X_{eas})$	
Muscovite	$X_{Al}^{VI} - 2$	$X_{ms}^2 (2 - X_{ms})$	Ideal mixing
Celadonite	$X_{Mg} / (X_{Al}^{VI} - 2 + X_{Mg} + X_{Fe})$	$\frac{1}{4} X_{cel} (2 - X_{ms})^2$	
Fe-celadonite	$X_{Fe} / (X_{Al}^{VI} - 2 + X_{Mg} + X_{Fe})$	$\frac{1}{4} X_{Fec} (2 - X_{ms})^2$	
Clinochlore	$1 - X_{ame} - X_{dap} - X_{Mnc}$	$(X_{cch} + X_{ame})^4 X_{cch} (1 + X_{ame})(1 - X_{ame})$	Symmetric regular solution model, W from Holland and Powell (web)
Amesite	$X_{Al}^{VI} - 1$	$\frac{1}{4}(X_{cch} + X_{ame})^4 X_{ame} (1 + X_{ame})^2$	
Daphnite	$\left(X_{Fe} / (X_{Mg} + X_{Fe} + X_{Mn})\right)\left((5 - X_{ame})/5\right)$	$X_{dap}^5 (1 + X_{ame})(1 - X_{ame})$	
Mn-chlorite	$\left(X_{Mn} / (X_{Mg} + X_{Fe} + X_{Mn})\right)\left((5 - X_{ame})/5\right)$	$X_{Mnc}^5 (1 + X_{ame})(1 - X_{ame})$	
Clinozoisite	$X_{Al} / (X_{Al} - 2 + X_{Fe^{3+}})$	X_{czo}	Ideal mixing
Pistacite	$X_{Fe^{3+}} / (X_{Al} - 2 + X_{Fe^{3+}})$	X_{ptc}	
Albite	$X_{Na} / (X_{Na} + X_{Ca})$	X_{ab}	$\gamma_{ab} = 1$
Anorthite	$X_{Ca} / (X_{Na} + X_{Ca})$	X_{an}	$\gamma_{an} = 6.7$
Water		Fugacity polynomial from Holland and Powell (1990)	

Table 6-3. Activity-composition relationships used in this study based on molar fraction of mineral end-members.

garnet. Detailed activity-composition relationship of garnet has been proposed by many authors (e.g., Ganguly and Saxena, 1984; Bermann, 1990; Ganguly et al., 1996). The model of Bermann (1990) seems to be one of the most widely applied during the 1990's. The asymmetric regular solution model of Ganguly et al. (1996), which modified and revised the Bermann (1990)'s model based on experimental data, is used in this study (table 6-4).

6-4-2. Biotite and chlorite

Biotite and chlorite are treated as quaternary solid solutions, involving Fe, Mg, and Mn end-members plus Tschermak's substitution ($Al^{IV}Al^{VI} \leftrightarrow MgSi$, etc). Four end-members of biotite are phlogopite, eastonite, annite, and Mn-biotite, and those of chlorite are clinochlore, amesite, daphnite, and Mn-chlorite. Mn end-members were included in the calculation frame in order to control the behavior of spessartine in garnet. Ideal part of activity of each end-member was formulated considering mixing on site.

Available models are formulated assuming no selective occupancy of Fe, Mg, or Mn between two distinct groups of six-coordination sites (M1 and M2 sites). In this study, however, preferential cation incorporation was adopted. This treatment was necessary because Tschermak's substitution is represented only by Mg end-members. All Al^{VI} had to be considered to correspond to Mg end-members. With this assumption, it was made possible to formulate the ideal part of the activity with molar fractions of end-members (fig.6-3). Validity of this formulation will be discussed later. Further selective incorporation of Al into one of the M2 sites (M2B site) was assumed for chlorite according to Holland et al. (1998).

i-j	W_{i-j} (J / mol)
Phl-Eas	10000
Phl-Ann	9000
Phl-Mnb	0
Eas-Ann	-1000
Eas-Mnb	-1000
Ann-Mnb	0

Table 6-5 Margules parameters for the symmetric solid solution model of biotite taken from Holland and Powell (Web Page).

i-j	W_{i-j} (J / mol)
Cch-Ame	18000
Cch-Dap	2500
Cch-Mnc	0
Ame-Dap	13500
Ame-Mnc	13500
Dap-Mnc	0

Table 6-6 Margules parameters for the symmetric solid solution model of chlorite taken from Holland and Powell (Web Page).

Biotite and chlorite are both assumed to behave as symmetric regular solutions. Margules parameter for each binary mixture is taken from Holland and Powell (1998; web page) (table 6-5, 6-6). Thermodynamic properties of Mn-biotite and Mn-chlorite are derived assuming ideal mixing with Fe and Mg end-members in the data set. Consequently, Margules parameters relating Mn end-members and Fe or Mg end-members were set to zero. Excess free energy of Tschermak's substitution involving Mn end-members was assumed to be the same as Fe end-members. For instance, $W_{eas\text{-}ann}$ (Margules parameter for eastonite-annite binary) is applied also for eastonite-Mn-biotite binary.

6-4-3. Muscovite

Muscovite is treated as a ternary solid solution. The three end-members are muscovite, celadonite, and Fe-celadonite. Cation exchange between muscovite and the other two end-members are Tschermak's substitution.

Holland and Powell (1998) states that ideal mixing can be assumed for muscovite as long as their activity model is applied. Selective incorporation of Fe and Mg cations into one particular six-coordination site is assumed according to their model.

6-4-4. Epidote

Epidote is treated as a binary solid solution involving Fe^{3+}-Al exchange. Fe^{3+} is assumed to occupy one particular site within the three Al sites. Epidote found in the Sambagawa pelitic schists are generally low in Fe^{3+} content. As long as the Fe^{3+} content is moderate and does not overflow into the second site, mixing of epidote can be assumed to take place at one site. This binary system is known to act as a nearly ideal solid solution (Holland and Powell, 1998).

6-4-5. Plagioclase

Cation exchange between anorthite and albite ($CaAl \leftrightarrow NaSi$) is treated as coupled substitution, considering local charge balance. Activity coefficient of anorthite had to be newly determined, since anorthite content of plagioclase in the study area is considerably low, typically less than 2 %. This composition range is on the albite-richer side of the generally observed peristerite gap, and is far out of the effective range of the plagioclase activity models that were previously proposed (Kerrick and Darken, 1975; Holland and Powell, 1992). For the Sambagawa high grade rocks, the miscibility gap at 500 °C is estimated to be 2 % to 20 % (Enami, 1981; Maruyama et al., 1982) in anorthite molar fraction.

Determination of activity coefficient was carried out assuming a

symmetric excess free energy at the composition range of the peristerite gap. Symmetric regular solution model was applied to a virtual solid solution, the two end members being pure albite (X_{An} = 0 %) and a virtual end member of X_{An} = 20 %:

$$G_{excess} = X_{An}(0.2 - X_{An})W_{Ab\text{-}An}$$

Activity coefficient was calculated assuming that the unmixing range starts at X_{An} = 2 % at 500 °C. In this case, gradient of total Gibbs free energy (G_{ss}) at X_{An} = 2 % and at X_{An} = 10 % (maximum of excess free energy) should be the same:

$$\left.\frac{\partial G_{ss}}{\partial X_{An}}\right|_{An2} = \left.\frac{\partial G_{ss}}{\partial X_{An}}\right|_{An10}$$

There is no need to care for the anorthite-richer side of the peristerite gap, since actual plagioclase composition never gets over the gap in the study area. Calculated activity coefficient was 6.7 at X_{An} = 1 %. The counterpart for albite is set to 1. This value is used in all thermodynamic calculations in this study.

6-4-6. Others

Pure phases were assumed for quartz, which seems quite reasonable. Paragonite contains minor amount of K, though it is generally less or around 3 % in molar fraction and shows no systematic change. Activity of paragonite was fixed to 0.97.

Pressure of H_2O is assumed to be equal to the environmental pressure (P_{rock}). Polynomial for H_2O fugacity (table 6-7) was taken from Holland and Powell (1990).

a1	-40338
a2	1.6474
a3	-0.0000062115
a4	2006800
a5	56292900
b1	117.372
b2	0
b3	0
b4	467100
b5	0
b6	0
c1	-0.0073681
c2	0.000000110295
c3	-987.74
c4	-0.784845692
c5	8.2948
c6	83366.7

$$RT \ln f = a + bT + cT^2$$

$$a = a_1 + a_2P + a_3P^2 + a_4P^{-1} + a_5P^{-2}$$

$$b = b_1 + b_2P + b_3P^{-1} + b_4P^{-2} + b_5P^{-1/2} + b_6P^{-3}$$

$$c = c_1 + c_2P + c_3P^{-2} + c_4P^{-1/2} + c_5P^{-1} + c_6P^{-3}$$

Table 6-7
Polynomial for the fugacity of H_2O from Holland and Powell (1990).

6-5. Reactions

Number of independent variables and constraints are summarized in table 6-8. Biotite-bearing system has 9 phases that consist of 10 system components. Total number of phase components is 22, 3 of which being fixed (paragonite, quartz, and H2O activity). Degree of freedom is 3 for this system according to the Gibbs phase rule. Garnet end-member concentration data provides 3 independent variables required.

Biotite-free system comprises 8 phases with 10 system components. Degree of freedom is 4 in this system, which requires another variable to be given in addition to garnet composition. Plagioclase composition is fixed in this study. It seems realistic, since anorthite content is known not to largely fluctuate in the study area. The validity of this assumption will be discussed in later section.

	Biotite-bearing	Biotite-free
Phases	9	8
Phase components	22	18
System components	10	10
Degree of freedom	3	4
Variables	21	17
Thermodynamic constraints (reactions)	12	8
Stoichiometric constraints	6	5
Total constraints	18	13

Table 6-8. Number of variables and constraints for biotite-bearing and biotite-free systems.

Independent reaction sets were obtained using the popular algorithm of linear algebra (Spear, 1989b). It was first applied in this field by J. B. Thompson Jr. (1982). Each phase component is expressed in terms of system components,

which can be treated as a matrix in the same way as linear simultaneous equations. By modifying the matrix, a set of independent stoichiometric relations between phase components is derived. Numerous combinations of reactions are possible. Reaction sets having least contribution from anorthite and fluid (water) was chosen for this study. Anorthite is generally very small in

Biotite-bearing system

	Net transfer reaction
(1)	2 Phl + Ms + 6 Qtz = Prp + 3 Cel
(2)	Pg + 2 Czo + 2 Qtz = Ab + 4 An + 2 Water
(3)	Ame + Cch + 4 Qtz = 3 Prp + 8 Water
(4)	Phl + 2 Pg + 3 Qtz = Prp + Ms + 2 Ab + 2 Water
(5)	4 Grs + 5 Pg + 6 Qtz = 6 Czo + 5 Ab + 2 Water
	Exchange reaction
(6)	Phl + Ms = Eas + Cel
(7)	Sps + Ann = Alm + Mnb
(8)	5 Sps + 3 Dap = 5 Alm + 3 Mnc
(9)	Alm + Phl = Prp + Ann
(10)	5 Alm + 3 Cch = 5 Prp + 3 Dap
(11)	Alm + 3 Cel = Prp + 3 Fec
(12)	Phl + Ame = Eas + Cch

Biotite-free system

	Net transfer reaction
(1)	Pg + 2 Czo + 2 Qtz = Ab + 4 An + 2 Water
(2)	4 Grs + 5 Pg + 6 Qtz = 6 Czo + 5 Ab + 2 Water
(3)	Ame + Cch + 4 Qtz = 3 Prp + 8 Water
(4)	2 Pg + 3 Dap + 6 Qtz = 5 Alm + 2 Ab+ 14 Water
	Exchange reaction
(5)	5 Sps + 3 Dap = 5 Alm + 3 Mnc
(6)	5 Alm + 3 Cch = 5 Prp + 3 Dap
(7)	Alm + 3 Cel = Prp + 3 Fec
(8)	Cel + Ame = Ms + Cch

Table 6-9. Independent reaction sets for biotite-bearing and biotite-free systems used in this study.

amount, so that too much control from anorthite content might lead to large propagated error. On the other hand, mol fraction of water in fluid phase is assumed to be 1 but is difficult to estimate the exact value. To minimize the potential error due to the fluid influence, it was essential to use reaction sets with less water participation.

6-6. Implementation of differential thermodynamic method

Calculation of differential thermodynamic method proceeds as follows:

(1) Fix starting values for every variable (temperature, pressure, and mineral compositions).

(2) Calculate every coefficient required for the linear equations describing the system.

(3) Calculate the difference of monitor parameters between the starting and the next values (change of garnet composition from the starting point to the next point).

(4) Give the values obtained in (3) and solve the simultaneous equations for changes of all other variables.

(5) Add obtained changes to the starting values, to get the new "starting value" for the next step.

(6) Iterate steps (2) to (5) until the core or the rim of garnet.

In this way, pressure and temperature history is calculated successively. Composition of minerals that once existed simultaneously keeping equilibrium must be used as the starting values, as well as proper pressure and temperature. Starting point can be either garnet rim (+ matrix minerals) or inside the grain (+ inclusion minerals). It is likely, though, that the observed

matrix minerals were modified after the termination of garnet growth. There are evidences such as sector zoning as described before. Chemical compositions of inclusion minerals within garnet grains are more reliable as starting values. Inclusion minerals that locate close to each other were analyzed and used as the starting data set, together with the garnet composition nearby.

Geothermobarometry in this and previous studies indicated that the recorded condition at the garnet rim is around 520 °C and 9 kbars. Calculation was adjusted so that the obtained P-T path achieves this standard P-T at the garnet rim. Provisional temperature and pressure were given for the starting point in the first calculation. Calculated temperature and pressure for garnet rim were compared to the standard value. If they did not coincide, starting temperature and pressure were altered and calculation repeated until desired value is worked out.

Samples used for the calculations are shown in table 6-10. Actual calculations were carried out, starting from interior points of the grain toward the core and the rim. The thermodynamic properties and the activity-composition relationships described in the previous section were considered completely. Temperature calibration for enthalpy and entropy was also incorporated using heat capacity. Temperature and pressure dependence of mineral molar volume was ignored. Linear simultaneous equations were solved with Gauss-Jordan method.

Sample	Mineral assemblage	Garnet zoning	
F2205	Bt-free→Bt-bearing	Normal(Ca-rich)	–
F2302	Bt-free	Normal(Ca-rich)	–
F2303	Bt-free	Normal(Ca-poor)	*, #
F0201	Bt-free	Normal(Ca-poor)	#
F0702	Bt-free	Normal(Ca-rich)	–
F0801	Bt-free	Composite	*
F1401	Bt-free	Normal(Ca-poor)	*, #
F1403	Bt-free	Normal(Ca-poor)	#
F2903	Bt-free	Composite	–
F3201	Bt-free	Composite	–

Table 6-10. List of samples used for the P-T calculation by differential thermodynamic method.
* : Sector zoning is present in the sample,
# : thin overgrowth is observed at the outer most rim of garnet grains.

6-7. Results

6-7-1. Ca-rich normal zoning

Both biotite-bearing sample (F2205) and biotite-free samples (F2302, F0702) indicated heating and compression throughout the garnet growth from the core to the rim (figs.6-1 and 6-2). Overall compression for Ca-rich normal zoning is 2 - 3 kbar in response to heating of 50 - 70 °C. Average dP/dT is around 4 - 5 kbar/100 °C. Outer portion of garnet grains where grossular decreases tends to indicate smaller dP/dT than the inner portion with grossular increase.

Calculation for sample F2205 was carried out assuming that biotite was present keeping equilibrium with the outer portion of garnet, defined by the appearance of inclusion biotite.

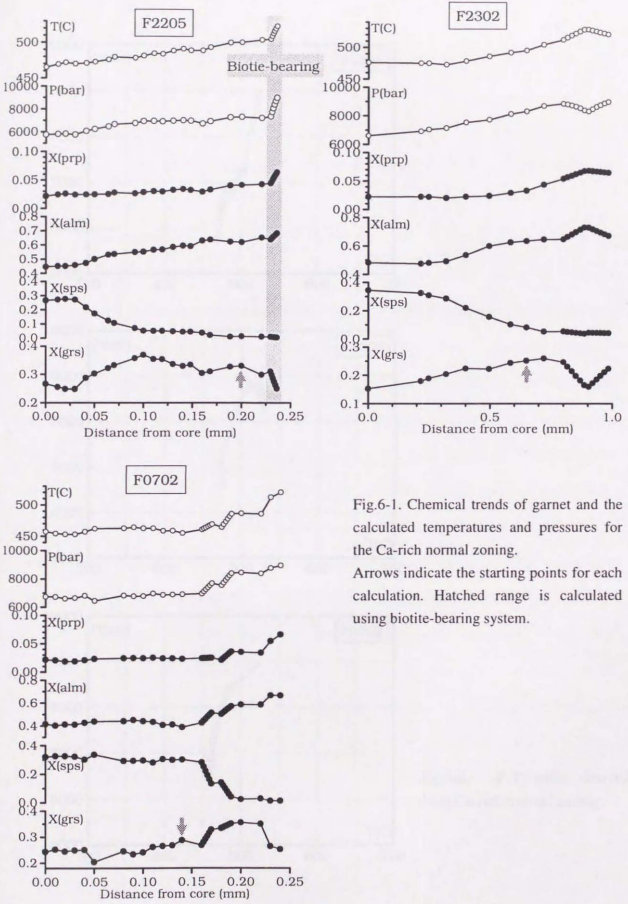

Fig.6-1. Chemical trends of garnet and the calculated temperatures and pressures for the Ca-rich normal zoning.
Arrows indicate the starting points for each calculation. Hatched range is calculated using biotite-bearing system.

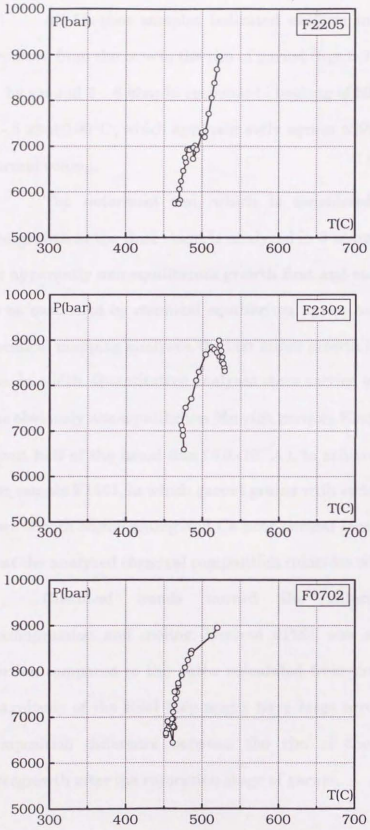

Fig.6-2. P-T paths derived from Ca-rich normal zoning.

6-7-2. Ca-poor normal zoning

All Ca-poor samples indicated uniform increase of temperature and pressure from the core to the rim of garnet (figs.6-3 and 6-4). Pressure increase d by around 3 – 4 kbar in response to heating of 50 – 60°C. Derived dP/dT is 4 - 5 kbar/100°C, which approximately agrees with the P-T path from Ca-rich normal zoning.

The outermost rim, which is considered to be the record of an overgrowth at the final stage, is analyzed in 3 samples of this category. There is an apparently non-equilibrium growth first and only the outermost rim seems to be controlled by chemical equilibrium again. According to two-dimensional chemical mapping analyses, the last minor growth in equilibrium was only 5-20 μm in width. Quantitative analyses were carried out carefully not to measure the obviously non-equilibrium Mn-rich portion. Electron beam was weakened to about half of the usual flux (6.0×10^{-9} A), to achieve higher spatial resolution. For sample F1401, in which garnet grains with sector zoning coexist, outermost part of both sector zoning and Ca-poor normal zoning was analyzed to confirm that the analyzed chemical composition coincides with each other.

Chemical trends toward the outermost growths indicated decompression and cooling. Derived dP/dT was smaller for the overgrowth portion compared to the paths calculated from the main normal zoning. The magnitude of the final step might have large error, because there is a large composition difference between the rim of the normal growth and the overgrowth after the resorption stage of garnet.

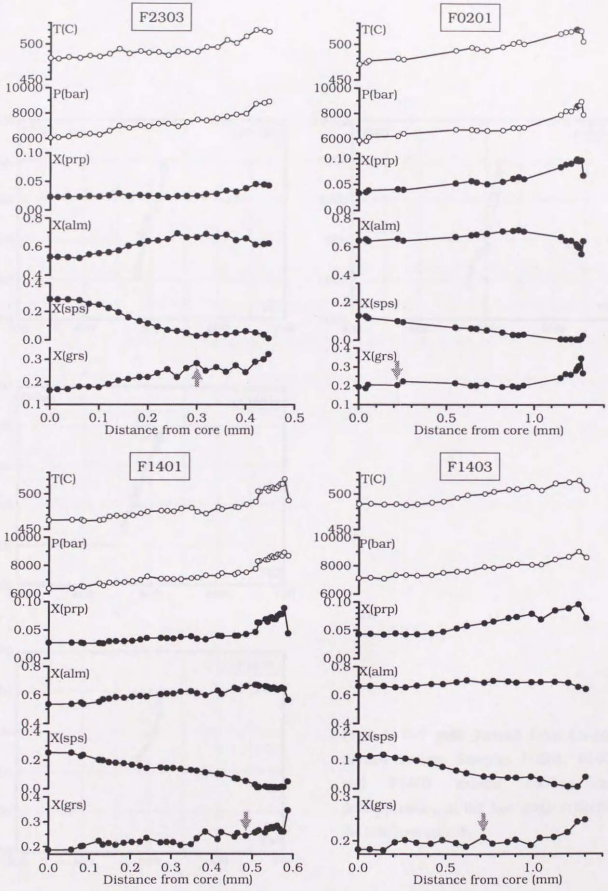

Fig.6-3. Chemical trends and the calculated temperatures and pressures for garnet with Ca-poor normal zoning. Arrows indicate the starting points for each calculation.

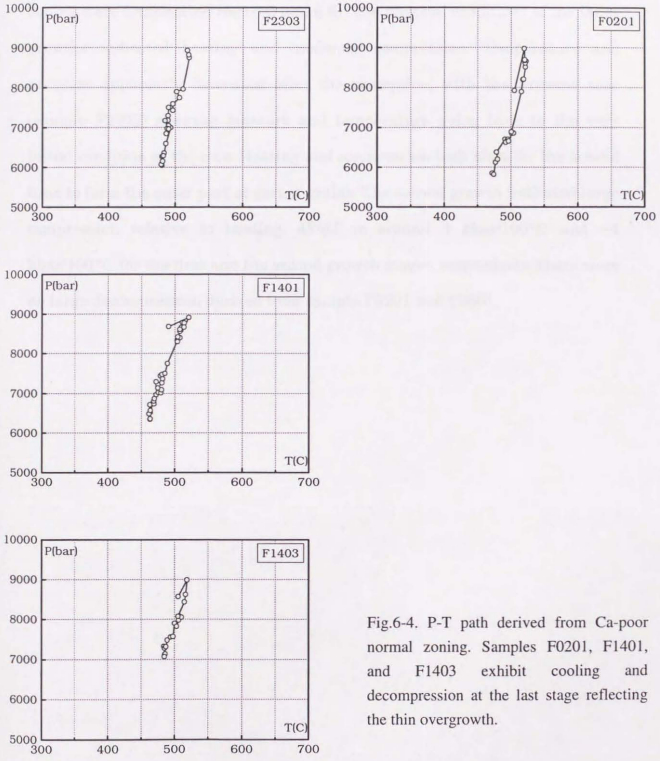

Fig.6-4. P-T path derived from Ca-poor normal zoning. Samples F0201, F1401, and F1403 exhibit cooling and decompression at the last stage reflecting the thin overgrowth.

6-7-3. Composite zoning

The pressure-temperature histories calculated from the composite zoning were complicated (figs.6-5 and 6-6). The physical conditions of the inner growths indicated heating and moderate compression. Temperature and pressure apparently decreased after the resorption, with the extreme case (sample F2903) showing pressure and temperature going back to the very initial condition at the core. Heating and compression took place for the second time to form the outer part of garnet grains. The second growth indicated large compression relative to heating. dP/dT is around 3 kbar/100°C and ~4 kbar/100°C for the first and the second growth stages, respectively. There were no large decompression derived from sample F3201 and F0801.

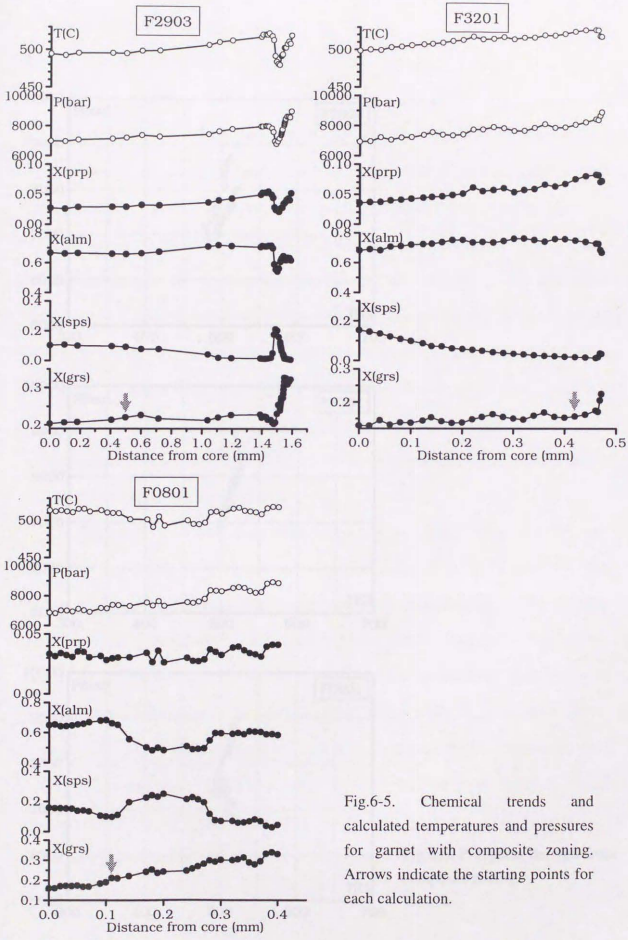

Fig.6-5. Chemical trends and calculated temperatures and pressures for garnet with composite zoning. Arrows indicate the starting points for each calculation.

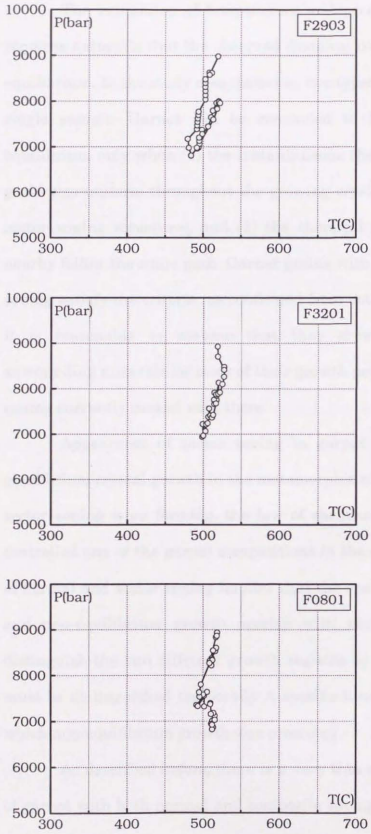

Fig.6-6. P-T paths derived from composite zoning.

7. Growth history of garnet

7-1. Equilibrium or non-equilibrium ?

The estimation of temperature and pressure from the garnet zoning requires naturally that the observed chemical compositions achieved chemical equilibrium. In the study area, however, two types of zoning pattern appear in a single sample. Garnet can be concluded to have grown under chemical equilibrium only when (1) the instantaneous chemical composition of a single grain was uniform throughout the growing crystal surface (i.e., not exhibiting sector zoning structure), and (2) the chemical composition trends of grains nearby follow the same path. Garnet grains with normal zoning and composite zoning satisfy the criteria, as confirmed from detailed chemical analyses. Thus it is reasonable to assume that they grew keeping equilibrium with surrounding minerals for most of their growth period, even if grains with sector zoning currently coexist with them.

Appearance of sector zoning in garnet is a solid evidence for non-equilibrium crystal growth in the metamorphic rocks. When garnet grains with sector zoning were forming, the law of chemical equilibrium could not have controlled any of the garnet compositions in the same sample. The coexistence of normal and sector zoning implies that the spatial occurrence of equilibrium and non-equilibrium growth overlap with each other. It is impossible to distinguish the two different growth regimes by the locations. Therefore they must be distinguished temporally. A specific time period must be identified in which non-equilibrium growth was promoted.

As described before, there is a very thin overgrowth texture at the rim of garnet with both normal and composite zoning. This texture often occurs in

samples where sector zoning is formed. Chemical mapping analysis with high spatial resolution has shown that the rim composition of thin overgrowth and that of coexisting sector zoning finally coincide with each other, at the outermost 5 to 20 μm. This agreement shows that the very rim of the two groups of garnet formed under equivalent condition, thereby suggesting simultaneous growth. It seems that the garnet composition was chemically controlled at that time, and most likely, almost satisfying chemical equilibrium. On the contrary, the inner part of sector zoning cannot have grown under equilibrium, because they exhibit intrasectoral inhomogeneity. The initial portion of the thin overgrowth onto the normal and composite zoned garnet grains often has extremely high Mn content, suggesting that it also deviates from equilibrium composition.

It is suggested from the above observations that the rim of garnet grains with sector zoning grew at the same time when the last minor overgrowth of garnet with normal and composite zoning occurred. The fact that the overgrowth is minor in volume is consistent with the tiny size of the grains exhibiting sector zoning. It seems that the total volume of garnet growth at the stage was small.

The shape of the garnet grains is another evidence to distinguish the time for the growth of non-equilibrium garnet. Larger garnet grains with normal or composite zoning are generally not perfectly euhedral, indicating resorption to some extent. The supposed non-equilibrium overgrowth occurs onto the resorbed shape of the grains. It is not likely that the sector zoned garnet grains survived the resorption stage, since they are very small in volume. It is thus obvious that, not only the growth of the rim, but also the nucleation of the grains with sector zoning postdated the growth and resorption of the grains with normal and

composite zoning.

A probable period for the occurrence of non-equilibrium garnet growth was constrained. The composition of garnet was chemically controlled under equilibrium with the environment, except the final short period of the garnet growth stage.

7-2. Formation of sector zoning

Formation of sector zoning is not under chemical equilibrium condition, but is controlled by kinetic factors. The primary evidence for kinetic control is the inconsistent chemical composition at each particular growth surface. In this paper, the term "sector zoning" refers to all tiny grains crystallized with irregular chemical compositions. There are grains in which intrasectoral heterogeneity is not obvious, though the chemical compositions differ from one grain to another. It is probable that they grew under non-equilibrium condition and nearly formed sector zoning, but the tendency was weak and did not create observable inhomogeneities. All of those grains are considered to be kinetically controlled during their growth.

Many of the previous studies ascribe the formation of sector zoning to relatively rapid crystal growth. Rapid crystal growth promotes "improper" cations to be incorporated into the crystal, thus the resulting chemical composition deviates from equilibrium. It must be noted though, that the "rapidness" in this case is a relative term.

Simple rapid heating does not explain the heterogeneity within each crystal surface. Growth rate must differ from one part to another of the crystal

surface, in order to create intrasectoral heterogeneity. One of the proposed mechanisms is that slightly curved growing surface incorporates different preferable cations according to its deviated angle from the ideal surface (Kitamura et al., 1993). When crystals are forced to grow rapidly, the ideally flat crystal surfaces often start to curve inward, making the corners more acute. This is called hopper growth. In this case, areas near the corners grow faster and will have higher step density. Non-ideal cations are incorporated in higher abundance compared to the flatter central areas of the crystal surfaces.

There are some garnet grains that show more than one domains within a crystal surface that have irregular chemical composition. Hopper growth cannot explain this inhomogeneity. On the other hand, characteristic surface structures might have caused abnormal growth on the flat surface. For instance, spiral growth or growth hillock (Paquette and Reeder, 1990). If this was the case, several domains in the flat surface can deviate from the equilibrium composition. It seems the latter hypothesis to be more realistic as long as the garnet in this study is concerned.

Similar sector zoning has been observed in skarn garnet, cause of which is suggested to be the unmixing in the garnet solid solution (Jamtveit et al., 1995), though the composition range for unmixing is not established yet. The chemical composition of skarn garnet is described mainly by grossular and andradite ($Ca_3Fe^{3+}_2Si_3O_{12}$), which is much different from the garnet considered in this study. It is confirmed by many experimental studies and also by observations of natural specimens that there is no unmixing in the quaternary system of pyrope, almandine, spessartine, and grossular within temperature and pressure of

geological interest. It is not likely that the immiscibility is the mechanism responsible for the growth of sector zoning.

Whatever the mechanism, the population density of garnet grains with sector zoning suggests that there was relatively large overstepping of temperature compared to material transfer. The number of garnet grains counted on the thin section is approximately $\leq 3\times10^3$ grains/cm^2 and ≤ 4 grains/cm^2 for the sector and normal zoned grains, respectively. Garnet grains with sector zoning occur with high nucleation density, often concentrated in a layer with 2 to 5 mm in width. It is suggested from a mesoscopic study (Skelton, 1997) that heavy material transfer promotes existing grains to grow faster rather than to nucleate another. On the contrary, nucleation rate increases in the case that material transfer is limited. High nucleation rate, together with the fact that the grains are locally clustered, suggests that the rate of material transfer at the time of non-equilibrium growth was small. Therefore it is possible that a moderate temperature increase was enough to produce a relatively large overstepping.

All previous descriptions about the sector zoning of garnet are from the periphery of the Tonaru or the Iratsu metagabbro masses (Shirahata and Hirajima, 1995). It has been thought that those rock masses drastically heated the surrounding pelitic schists to form contact aureole. However, the P-T conditions for the supposed non-equilibrium overgrowth at the outermost rim of garnet was lower than the peak metamorphic temperature and pressure, according to the calculation in this study (fig.6-4). Together with the fact that sector zoning occurred at a location far from any of the tectonic blocks (e.g., sample J3015 in fig.3-17), it is not likely that those rock masses were the heat sources for the non-

equilibrium garnet growth.

It is more probable that sector zoning was formed after the peak metamorphic condition was achieved. An episodic temperature reversal during the retrograde stage may be sufficient to form sector zoning, if the material transport rate is very small.

7-3. Record of the emplacement

Excluding the growth under non-equilibrium condition, temperature and pressure trends recorded by growing garnet were deduced using differential thermodynamic method.

From many previous studies concerning garnet zoning, it is known that both the Ca-poor and the Ca-rich normal zoning are common in the Sambagawa metamorphic belt. Grossular content in the typical garnet from the albite-biotite zone initially increases from the core, and then decreases toward the rim, just as the Ca-rich normal zoning. Garnet grains with similar chemical trends to the Ca-poor zoning are commonly found in the oligoclase-biotite zone of Besshi district. Rocks bearing Ca-rich and Ca-poor type garnet are both ordinary pelitic schists.

P-T paths derived from the two types of normal zoning indicate similar histories of heating and compression from beginning to end. Temperature increases by 50 to 70 °C while pressure increases by 2 to 3 kbar, with overall dP/dT approximately 3 to 4 kbar/100 °C. It is likely that the Ca-rich and the Ca-poor normal zonings are both the product of the regional Sambagawa metamorphism. The reason of the difference in grossular content is not clear. Judging from the fact that each zoning occurs in schists from particular metamorphic grade, either P-T

conditions or compositions of matrix minerals at the early stage of garnet growth may have played a role.

Composite zoning, on the other hand, probably records the disturbance caused by the emplacement of the Iratsu metagabbro mass. Derived P-T paths for composite zoning have two distinct stages of heating and compression. First and second prograde paths are discontinuous. Resorption texture is observed between the two prograde growths, when temperature (and pressure, for sample F2903) decreases according to the calculation results. It seems as if an overall prograde P-T path is interrupted in the midst. Grains with composite zoning only occurred in the vicinity of the tectonic blocks. It is most likely that the emplacement of the Iratsu metagabbro is responsible for the interruption of the prograde growth of garnet.

Considering that the composite zoning always starts from Ca-poor core, it is suggested that composite zoning is a kind of mutated Ca-poor normal zoning. That is, whatever the event may be that interrupted the growth, the influence of the event reached only on the garnet grains with Ca-poor normal zoning. The relation probably implies the spatial configuration of the rocks during the subduction process.

There is evidence that indicates the nature of the disturbance. It was noted in the previous chapter that some samples contain two types of garnet. Both exhibit composite zoning, but the chemical composition of the earlier (inner) zoning is clearly different from each other. Two chemical trends converge into the same chemical composition for the later (outer) zoning. Chemical composition of chlorite in the matrix is uniform within each sample. It is suggested from the

chemical trend, that the two types of garnet came together after their first prograde growth. The coexistence of layers with apparently different bulk chemistry in those samples supports the view that the rocks were subject to mechanical mixing. They grew in two different bulk rock chemistries, most likely pelitic and basic compositions respectively, and were physically mixed with each other during the interruption period between the two prograde growths. It is reasonable that the mechanical mixing took place as a result of the ductile flow caused by the emplacement of the tectonic blocks.

The history of the studied pelites in the vicinity of the Iratsu metagabbro mass can be summarized as follows (fig.7-1): (1) Normal zoning was formed due to the Sambagawa metamorphism with high compression rate. (2) Growth of part of the grains with Ca-poor normal zoning was interrupted due to the emplacement of the Iratsu metagabbro mass. Garnet grains record evidences of resorption, cooling, partly decompression, and mechanical mixing. (3) Disturbed grains started growing again to form the second prograde zoning, maybe due to the Sambagawa regional metamorphism. The compression rate was higher than that of stage (1). (4) Minor non-equilibrium growth during the retrograde stage, probably under a higher pressure condition compared to the prograde path (anti-clockwise).

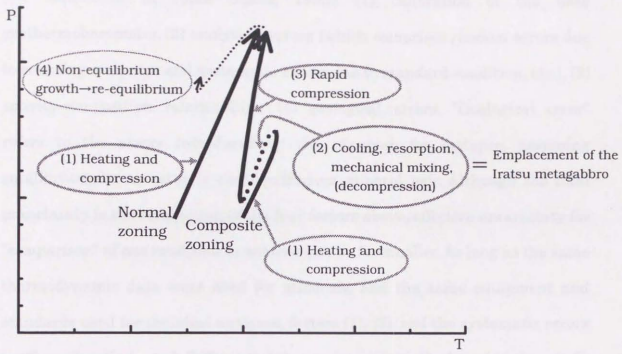

Fig.7-1. Summary of the deduced P-T histories of garnet growths.

8. Validity of the derived P-T paths

There are several factors that are known to cause uncertainties in the P-T estimation in rocks (Spear, 1993): (1) calibration of the used geothermobarometer, (2) analytical errors (which comprises random errors due to counting statistics and systematic errors due to standard condition, etc.), (3) activity-composition relationships, (4) geological errors. "Geological error" refers to the errors introduced by the observer, for instance, assuming equilibrium for an actually non-equilibrium mineral pair. Although the total uncertainty is the summation of the four factors above, effective uncertainty for "comparison" of one condition to another can be far smaller. As long as the same thermodynamic data were used for minerals, and the same equipment and standards used for chemical analyses, factors (1), (3), and the systematic errors in (2) can be eliminated. Differential thermodynamic method used in this study derives the relative change of temperatures and pressures. Two of the most influential factors in this study are the geological uncertainty and the random analytical uncertainty, which will be discussed below.

There are several sources of geological errors. The differential thermodynamic method assumes certain mineral assemblage to have existed keeping equilibrium throughout the time period of interest. If any of the assumed minerals were not in equilibrium at the time, the calculation is empty. Even if the existence of the minerals were confirmed, then the uncertainty arises from the analyzed mineral compositions, which do not always maintain the compositions in equilibrium. It is difficult to estimate the true chemical compositions at the condition of interest, since the studied samples exhibit evidences of retrograde reactions. Moreover, the chemical composition of

reactions. Moreover, the chemical composition of plagioclase is assumed to be constant in this study when biotite is not involved in the system. If plagioclase was greatly controlling the chemical behavior of the system, the assumption may lead to large error.

One way to estimate the validity of the calculation is to compare the calculated mineral compositions with the observed minerals. Differential thermodynamic method calculates the changes of compositions of minerals as well as temperatures and pressures. It is possible to compare the calculated and observed chemical compositions of minerals to judge whether the calculated composition changes are realistic or not.

Other uncertainties include the starting temperatures and pressures given for the calculation. It concerns the input data for the differential thermodynamic method. Potential error derived from fairly large perturbation of the initial temperatures and pressures as well as mineral compositions will be summarized applying the method of Kohn (1993).

Another source of error involving the activity-composition relationships in chlorite and biotite will be discussed. Finally, the difference between the model in this study and that in the previous study will be mentioned.

8-1. Supposed mineral assemblages

One can never be sure about whether all the minerals present in the matrix were in chemical equilibrium during metamorphism. The only means available for us today is to search for evidences of non-equilibrium behavior.

Biotite is found only closely associated with chlorite or in the cracks of

garnet in some samples. Such biotite is interpreted to be the product of retrograde reaction. Biotite can be excluded from equilibrium mineral assemblage.

Chlorite in the studied samples typically occurs as aggregates that are not participating the schistosity. The grains have random and often kinked stretching direction, which makes it difficult to estimate the accurate chemical composition of chlorite when in equilibrium with garnet rim. It is unreasonable, though, to assume that chlorite was absent during garnet growth. Chlorite is one of the main component minerals in the low grade zones of the Sambagawa metamorphic belt. It is supported by many authors that chlorite supplied materials for growing garnet. There are two types of chlorite in the Sambagawa pelitic schists (Higashino, 1975). One type is individual grains forming schistosity and is thought to be the chlorite having been in equilibrium during prograde metamorphism. Another type of chlorite is not concordantly aligned and is probably the product of the retrograde reaction. The former type rarely occurs in the study area. Even if it does, the expected difference of chemical composition is not clearly recognized, probably because the rim portion of the individual chlorite grains is also subject to the retrograde reaction. Maybe the retrograde metamorphism has substantially proceeded in the area, so that it altered the chemical composition of most chlorite grains present. Retrograde reaction is also suggested from the rounded shape of garnet.

Muscovite, paragonite, and epidote define the schistosity. No particular texture that indicates non-equilibrium was observed. Some epidote grains have cores enriched in light-rare-earth-elements (LREE), which implies that their nucleation took place at an early stage of metamorphism. Quartz and plagioclase

can be almost indisputablely assumed that they were present in equilibrium with garnet.

Another important check-point is to estimate whether the minerals were in equilibrium with garnet throughout its growth. Inclusion minerals in garnet grains indicate the existence of each mineral during garnet growth. Biotite inclusion does not appear within garnet crystals even in some of the biotite-bearing samples. It was assumed in this study that if no inclusion of biotite was observed, biotite did not exist during garnet growth. This assumption is consistent with the currently accepted view that biotite was not ubiquitously present during the Sambagawa prograde metamorphism.

There was only one sample that had biotite inclusion within garnet, and it was in the outer portion of the crystal (fig.8-1). The P-T calculation was carried out assuming biotite was present after the appearance of the biotite grain. It is still uncertain if the only analyzed biotite inclusion was truly included during the growth stage. There is always possibility that the examined inclusion mineral is formed later within a crack not observable in the direction of the thin section. When biotite is excluded from the system, the calculated pressure increase

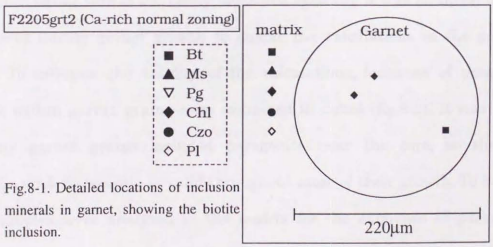

Fig.8-1. Detailed locations of inclusion minerals in garnet, showing the biotite inclusion.

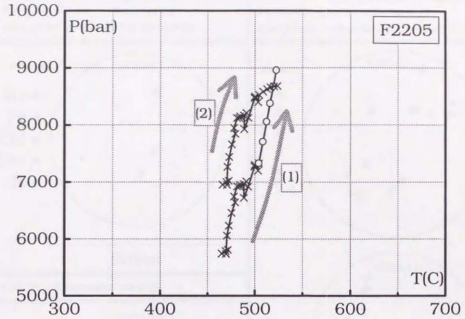

Fig.8-2. Comparison of P-T paths calculated (1) involving biotite near the rim and (2) totally biotite-free until the rim. Blank circles indicate the calculation results using the biotite-bearing system.

becomes smaller than that derived with biotite-bearing system, especially for the last stage where grossular decreases (fig.8-2). Although the extent of compression may become smaller, that of heating shows no large change in response to the modification of calculation frame. The overall dP/dT of the P-T path is still around 3 kbar/100°C.

Since paragonite is not easily identified optically, it was assumed to have been present during garnet growth to enable the calculations in the previous chapters. To estimate the validity of the calculations, locations of paragonite inclusions within garnet grains were examined in detail (fig.8-3). It was shown that many garnet grains included paragonite near the core, so that the assumption with paragonite is valid throughout most of their growth. To be sure, several samples were analyzed in the matrix for the existence of paragonite.

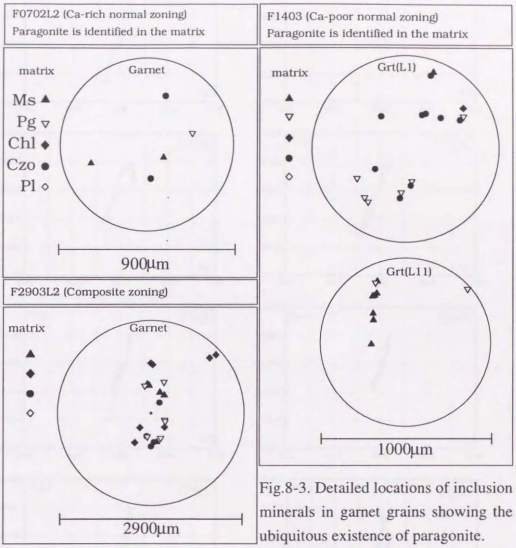

Fig.8-3. Detailed locations of inclusion minerals in garnet grains showing the ubiquitous existence of paragonite.

Paragonite was identified in samples F0702 and F1403. Paragonite must have been present with garnet, at least from the first appearance of the paragonite inclusion until the garnet rim. The P-T calculations are shown in figure 8-4, with emphasis on the results obtained from the data where paragonite was confirmed. No large difference is observed between the derived P-T paths for paragonite-bearing samples and those for the samples which analysis was not carried out in the matrix. The assumption for the presence of paragonite seems reasonable in the study area.

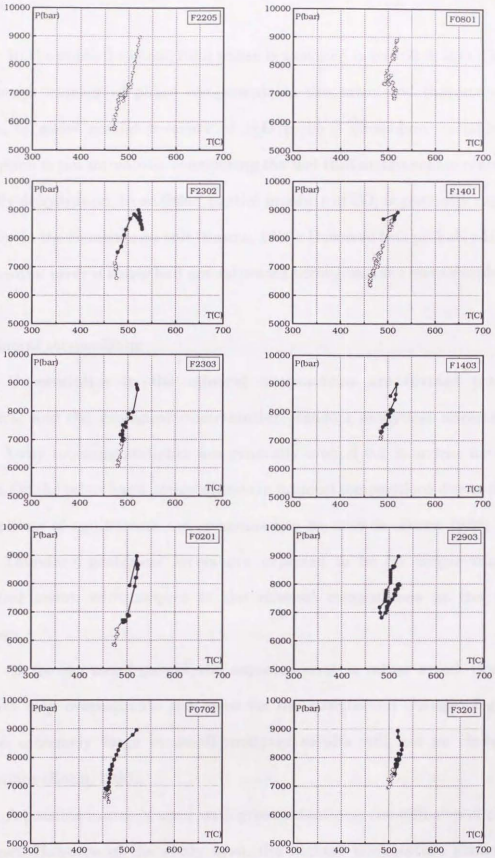

Fig.8-4. P-T paths showing the range where existence of paragonite was confirmed. Gray blank circles indicate the range before the first appearance of paragonite inclusion within garnet grains. Solid circles indicate the paths after the appearance of paragonite. Samples F0702 and F1403 contained paragonite in the matrix.

In the studied system, fluid phase is assumed to be 100 % H_2O. There is not enough number of phase components in the calculated thermodynamic system, to allow partial pressure of H_2O to be a dependent variable. The assumption is not unrealistic considering the fact that metamorphic reaction is basically dehydration. In addition, partial pressure of CO_2 is generally regarded to be low in the Sambagawa belt (Banno, 1986). However, this probably leads to the potential error if water had not saturated throughout the metamorphism.

8-2. Mineral compositions

Uncertainties in the mineral compositions are divided into the analytical and the geological uncertainties. Random analytical uncertainties due to X-ray counting statistics are generally around 0.5 % or less for major cations. On the other hand, uncertainties in mineral compositions due to invalid assumptions of equilibrium are considered to be $\pm$ 5 % (Ferry, 1980; Kohn, 1993). Therefore, geological errors are expected to be far larger than the analytical errors with respect to the mineral compositions at the initial condition.

As for the zoned garnet, the expected error is rather small. Counting statistics may overestimate the error for the composition change of garnet, because extremely large or small analyses results will not be chosen for calculations (Kohn, 1993).

A possible source of error with great potential is the diffusion of cations in garnet. However in the study area, the highest temperature achieved is around 520 °C, where the alteration of chemical composition due to diffusion is generally assumed to be very small. From chemical map analyses, it is obvious

that the euhedral shape of the growth surfaces is preserved as each isochemical contour line within the grains. It suggests that there had been no substantial diffusion of elements after the formation of zoning. Garnet from the oligoclase-biotite zone exhibited diffusion texture around quartz inclusions (fig.3-10 and 3-11). However, it is seen that the main chemical zoning from the garnet core to the rim is completely reserved within the grain. Considering the mass balance, it is reasonable to assume that the majority of the volume within the grain still maintains the chemical composition of growth zoning. Furthermore, it is clear from the chemical trend of the diffusion zone, that the diffusion took place only at the time when the rim of garnet was formed. The peak temperature achieved by the oligoclase-biotite zone schists is around 600°C. The temperature difference of 100°C may have caused drastic difference in the diffusional behavior of elements between the albite-biotite zone and the oligoclase-biotite zone. Again, garnet from the albite-biotite zone is not supposed to have altered after the growth. The influence of the diffusion is not considered in this study, because the amount seems to be small, and also because there is no sufficient data to estimate the diffusional influence in a low-temperature condition as in the study area.

As mentioned above, differential thermodynamic method derives changes in all involved variables besides temperatures and pressures. Examination of calculated composition changes for the other minerals helps excluding unrealistic solutions. The calculated and the observed mineral compositions are shown in figure 8-5 and 8-6.

There is only one sample calculated assuming biotite-bearing system. Biotite showed gradual increase of phlogopite content as the result of iterative

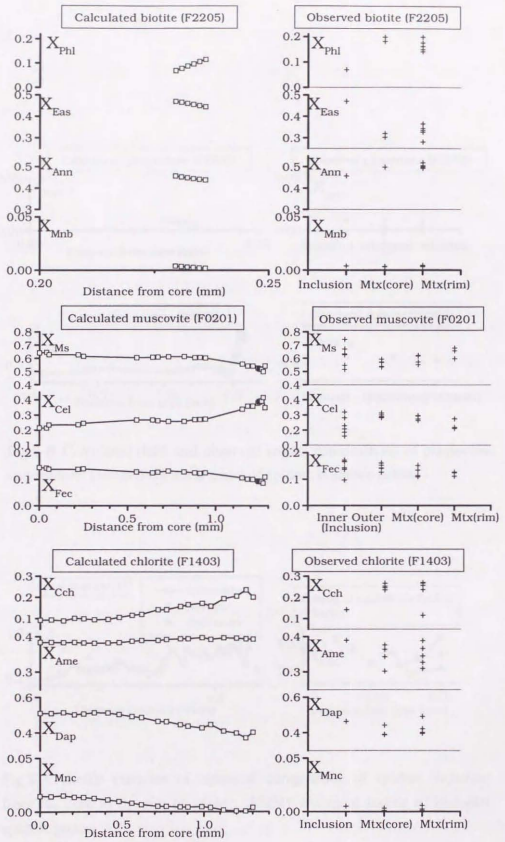

Fig.8-5. Calculated (left) and observed (right) compositions of biotite, muscovite, and chlorite. Observed compositions are classified into (1) inclusions, (2) core of matrix minerals, and (3) rim of matrix minerals. Muscovite inclusions are further classified into inner (inclusion near the garnet core) and outer (that near the rim) inclusions.

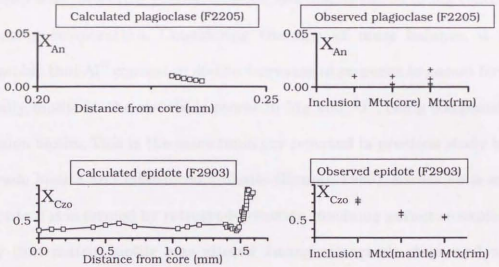

Fig.8-6. Calculated (left) and observed (right) compositions of plagioclase and epidote. Detailed chemical trend of epidote is shown below.

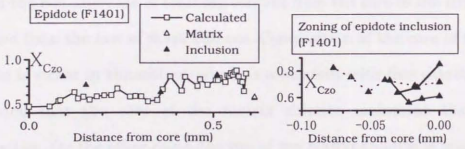

Fig.8-7. (Left): variation of chemical composition of epidote inclusion from the core to the rim of garnet. (Right): chemical zoning of included epidote grains.

calculation. Eastonite (Mg component to represent Tschermak's substitution) content was predicted to show minor decrease. Total Mg content increased and Al^{VI} content decreased toward garnet rim. This is consistent with the general tendency that coexisting garnet, chlorite, and biotite enrich in Mg content with increasing temperature. Considering the law of mass balance, it is also reasonable that Al^{VI} content in biotite decreases in response to garnet formation. Actually, biotite in the matrix is poorer in Mg and Al^{VI}, being compared to the inclusion biotite. This is the same tendency reported in previous study between prograde biotite and later-formed biotite (Enami, 1983). Excess Fe is expected in biotite if it is formed by retrograde reaction involving garnet resorption. It is likely that matrix biotite was altered during retrograde stage and no more maintains the composition in equilibrium with garnet.

Mg contents in chlorite also increase in the calculations (fig.8-5). Clinochlore increases in response to increase of pyrope content in garnet. Amesite content does not show large change, but has a tendency to decrease toward the rim. Increase of total Mg content from the core to the rim is just as expected from the law of mass balance. Composition of the core of the matrix chlorite is richer in clinochlore, which is consistent with this calculation. It is suggested that the core of the matrix chlorite maintains the prograde composition. On the other hand, the rim of the matrix chlorite is generally rich in Fe. Current composition of chlorite is suggested to have altered during retrograde stage. Their texture also displays their retrograde origin.

Mn content is low in natural chlorite. In case the content of Mn-chlorite got too high in the course of iterative calculation, it is suspected that the chosen starting composition was improper. Such results were in fact obtained in some

cases. They were regarded to invalid and another starting composition was chosen for each case. The calculations were retried until realistic Mn contents in chlorite were derived.

Calculated changes of muscovite compositions are consistent with the observed tendency of muscovite included in garnet grains in most cases. Calculated and analyzed celadonite contents increase and muscovite (end-member) contents decrease from the core to the rim of garnet (fig.8-5). Present muscovite (mineral) in the matrix exhibits chemical zoning with celadonite-poor rim. Decrease of celadonite is neither observed in the muscovite inclusion in garnet, nor predicted by the calculation. The celadonite-poor rim may be explained to be the product of retrograde reaction. Fe-celadonite content is maintained around 10 to 15 mol% both in the calculation result and in observed matrix muscovite.

Anorthite content in plagioclase is always less or around 2 mol%. It is constrained to extremely low values presumably because of the peristerite gap. The calculated anorthite content (only in the biotite-bearing system) decreases toward the rim of garnet, and does not fluctuate largely in the iterative calculation. It is consistent with the Ca-rich core observed in the matrix plagioclase (fig.3-29). Though there are Ca-rich parts found in the rim of plagioclase porphyroblasts, they are generally regarded as retrograde product. It seems that the calculation frame produces reasonable values for the plagioclase composition.

Epidote is the third Ca-bearing phase involved in the calculation. It is important to know the behavior of epidote in response to grossular content in garnet, since Ca end-members are thought to be sensitive to pressure change.

Calculated mole fraction of clinozoisite component roughly increased where grossular content in garnet increased, and decreased where grossular decreased (fig.8-6 and 8-7; for grossular trends, refer to fig.6-3 and 6-5). The tendency was the same between the biotite-bearing system (variable anorthite content) and the biotite-free system (fixed anorthite content). It shows that the fixation of anorthite content in plagioclase is being a proper constraint for the calculation.

The chemical composition in epidote is critical because the composition of epidote inclusion in garnet and that of matrix epidote is much different (fig.8-6). It is seen in figure 8-7, however, that the epidote grains included in garnet show complicated zoning patterns. The range of the compositional variation found in the epidote grains largely coinsides with the calculated variation. It is feasible that epidote had changed the chemical composition in response to the change of the environment.

It is known that zoisite forms at higher temperature phase in reality (Enami and Banno, 1980). Zoisite always contains smaller Fe^{3+} content than epidote (clinozoisite - pistacite) when the two epidote group minerals are in equilibrium. In the epidote-amphibolite facies condition, $Fe^{3+}/(Al+Fe^{3+})$ of zoisite is around 4 % in contrast with 12 % for epidote (according to the data from marginal part of the Iratsu mass: Enami and Banno, 1980). Though observed epidote can be identified as true epidote from its composition range, calculation results with too much clinozoisite content should be excluded as being unrealistic. In fact, some of the calculations produced unrealistically high clinozoisite content in epidote. Some of the samples with Ca-poor normal zoning or composite zoning produce very high clinozoisite content (less than 4 % of

$Fe^{3+}/(Al+Fe^{3+})$) corresponding to the most Ca-rich garnet composition. Zoisite might have formed at the time period during garnet growth in those samples. It is however impossible to confirm the existence of zoisite, even if it has survived included within garnet. Epidote inclusions are very small in size that there is no appropriate means to determine their crystallographic axis. In this study, calculations were carried out again using lower clinozoisite values as the starting compositions in those cases, to avoid unrealistic results. It is of course possible to involve zoisite formation into the calculation frame. However the potential error introduced by assumed zoisite formation would be even larger as long as the coexistence of zoisite is not yet confirmed in those samples. Furthermore, there is no large difference between the calculated P-T paths using epidote and zoisite. This is because the thermodynamic properties of zoisite and epidote are similar to each other. Unless there is substantial chemical influence caused by the coexistence of epidote and zoisite, the calculated P-T paths will be stable. Ca-rich normal zoning derives no unnatural compositions for epidote.

8-3. Influences of input data

The method to estimate the uncertainty for the P-T path derived by differential thermodynamic method was proposed by Kohn (1993). The standard equation of error propagation for the function $f(\alpha_1, \alpha_2, \cdots, \alpha_k, \alpha_l, \cdots, \alpha_n)$ is as follows:

$$\sigma_f^2 = \sum_{k=1}^{n} \sum_{l=1}^{n} \sigma_{\alpha_k} \sigma_{\alpha_l} \rho_{\alpha_k \alpha_l} \left(\frac{\partial f}{\partial \alpha_k} \right) \left(\frac{\partial f}{\partial \alpha_l} \right) \qquad (8\text{-}1)$$

σ_α is the uncertainty in each parameter, $\rho_{\alpha_k \alpha_l}$ is the correlation coefficient between α_k and α_l. In the differential thermodynamic method, it is impossible to evaluate the partial derivatives of the resulted ΔP or ΔT analytically. The numerical procedure proposed by Roddick (1987) was adopted to estimate the partial derivatives. The proposed method is to perturb the parameter in interest, and the partial derivative is approximated as follows:

$$\frac{\partial f}{\partial \alpha_k} \approx \frac{f(\alpha_k + \Delta\alpha_k) - f(\alpha_k)}{\Delta\alpha_k} \qquad (8-2)$$

Perturbing the value of input variables one at a time, and the partial derivatives of ΔP or ΔT with each variable are calculated. Giving proper uncertainties, the propagated error will be obtained from the equation (8-1).

P and T changes derived from the differential thermodynamic method can be expressed by the monitor parameters, using the Jacobian matrix coefficients (Spear, 1989):

$$\Delta T = \sum_{i=1}^{v} \left(\frac{\partial T}{\partial X_i} \right) \Delta X_i = \sum_{i=1}^{v} T'_{x_i} \, \Delta X_i \qquad (8-3)$$

$$\Delta P = \sum_{i=1}^{v} \left(\frac{\partial P}{\partial X_i} \right) \Delta X_i = \sum_{i=1}^{v} P'_{x_i} \, \Delta X_i \qquad (8-4)$$

where X_i are the monitor parameters, and T'_{x_i} and P'_{x_i} represents the partial derivatives of temperature and pressure with respect to X_i. Monitor parameters used in this study are the content changes of pyrope, almandine and grossular, which makes v = 3. Anorthite content will not be involved in this equation, because it is fixed and the given "change of anorthite content" is always zero. Applying the error propagation equation (8-1) to equations (8-3) and (8-4), the total propagated error is written as follows:

$$\sigma^2_{\Delta T} = \sum_{k=1}^{n}\sum_{l=1}^{n}\left(\sum_{i=1}^{v}\left(\frac{\partial T'_{X_i}}{\partial \alpha_k}\right)\Delta X_i \sigma_{\alpha_k}\right)\left(\sum_{j=1}^{v}\left(\frac{\partial T'_{X_j}}{\partial \alpha_l}\right)\Delta X_j \sigma_{\alpha_l}\right)\rho_{\alpha_k \alpha_l}$$

$$+\sum_{i=1}^{v}\sum_{j=1}^{v} T'_{X_i}\, T'_{X_j}\, \sigma_{\Delta X_i}\sigma_{\Delta X_j}\rho_{\Delta X_i \Delta X_j} \qquad (8\text{-}5)$$

$$\sigma^2_{\Delta P} = \sum_{k=1}^{n}\sum_{l=1}^{n}\left(\sum_{i=1}^{v}\left(\frac{\partial P'_{X_i}}{\partial \alpha_k}\right)\Delta X_i \sigma_{\alpha_k}\right)\left(\sum_{j=1}^{v}\left(\frac{\partial P'_{X_j}}{\partial \alpha_l}\right)\Delta X_j \sigma_{\alpha_l}\right)\rho_{\alpha_k \alpha_l}$$

$$+\sum_{i=1}^{v}\sum_{j=1}^{v} P'_{X_i}\, P'_{X_j}\, \sigma_{\Delta X_i}\sigma_{\Delta X_j}\rho_{\Delta X_i \Delta X_j} \qquad (8\text{-}6)$$

The first term on the right side of the equation estimates the uncertainty due to the initial condition data. The second term accounts for the uncertainty of the changes of the monitor parameters, ΔX_i. Uncertainties in the derived P-T path caused by the uncertainties of the input initial condition and the monitor parameters can be calculated using the equations (8-5) and (8-6).

Two different systems were assumed for the calculation in this study: biotite-bearing and biotite-free system. Therefore, the error propagation was attempted on two representative calculation steps to estimate the magnitude of the supposed uncertainties. One of the growth steps of garnet after the appearance of biotite inclusion in sample F2205 was examined as a representative step. For biotite-free system, calculation for Ca-poor normal zoning in sample F1401 was used.

First, T'_{X_i} and P'_{X_i} were calculated using the starting conditions. Partial derivatives in terms of each factor (T, P, X_i, entropy, and volume) were then derived perturbing each parameter and applying the equation (8-1). The partial derivatives derived for the calculation of biotite-bearing system are tabulated in table 8-1 as an example.

C	$\partial T'_{Xsm}/\partial C$	$\partial T'_{Xsm}/\partial C$	$\partial T'_{Xsm}/\partial C$	$\partial P'_{Xsm}/\partial C$	$\partial P'_{Xsm}/\partial C$	$\partial P'_{Xsm}/\partial C$	σ_C	$\sum[(\partial T'_{Xsm}/\partial C)\Delta x_i\sigma_{x_i}$	$\sum[(\partial P'_{Xsm}/\partial C)\Delta x_i\sigma_{x_i}$
T	2.172	0.123	-0.124	80.582	0.142	-14.254	25	0.2723	12.013
P	-0.042	0.003	0.008	0.078	0.022	-0.019	500	-0.1156	0.361
Xprp	-21678.665	137.154	135.441	-1790522.04	3131.658	474.195	0.0022	-0.1835	-15.038
Xalm	2635.927	-130.480	-18.478	189812.699	-43003.561	-33382.327	0.0128	0.1167	9.478
Xsps	1546.753	777.421	713.353	1447040.749	1377019.992	1367695.855	0.0004	0.0017	0.572
Xgrs	1361.247	85.088	-33.124	93642.347	-5233.871	-14752.558	0.0155	0.0987	7.575
Xphl	-96.128	5.181	-0.732	350926.757	-18912.642	2673.739	0.0069	-0.0022	7.920
Xeas	-55.994	2.234	-12.269	204412.079	-8157.202	44788.221	0.0470	-0.0022	8.114
Xann	67.876	-16.514	-0.386	-247788.269	60286.787	1408.063	0.0457	0.0053	-19.524
Xmnb	848.845	822.784	820.816	-3098797.014	-3003659.212	-2996475.121	0.0008	0.0006	-2.138
Xms	-41.157	2.855	6.754	150247.590	-10423.959	-24656.371	0.0278	-0.0059	21.597
Xcel	52.520	-4.596	-5.290	-191729.649	16779.720	19310.020	0.0144	0.0032	-11.739
Xfec	-4.575	1.796	-4.416	16699.835	-6555.818	16120.884	0.0078	0.0004	-1.471
Xpg	-12.817	-0.979	-0.131	-6886.342	-525.731	-70.514	0.0194	-0.0011	-0.586
Xcch	1733.547	-173.524	23.958	-123453.392	12357.400	-1706.172	0.0200	0.0962	-6.852
Xame	908.796	-83.205	45.603	-64719.321	5925.387	-3247.571	0.0311	0.0680	-4.842
Xdap	-1848.958	222.244	-15.050	131672.343	-15826.967	1071.759	0.0488	-0.2399	17.084
Xmnc	-14694.804	-13908.626	-13829.423	1046480.867	990493.745	984853.304	0.0001	-0.0021	0.147
Xczo	0.000E+00	-1.421E-11	5.143E-10	-1.455E-08	1.251E-09	-4.002E-08	0.0490	-3.080E-13	2.130E-11
Xpte	0.000E+00	1.421E-11	-5.143E-10	1.455E-08	-1.251E-09	4.002E-08	0.0510	3.211E-13	-2.221E-11
Xab	-152.399	16.703	76.770	-81878.145	-8973.867	41245.612	0.0198	-0.0268	-14.407
Xan	152.399	-16.703	-76.770	81878.145	-8973.867	-41245.612	0.0020	0.0027	1.472
Sprp	-2.166	-0.165	-0.022	-177.649	-13.562	-1.819	1.000	-0.009	-0.779
Salm	-2.508	-0.191	-0.026	-289.699	-22.117	-2.966	1.000	-0.011	-1.270
Ssps	-0.003	0.000	0.000	-4.341	-0.331	-0.044	1.000	0.000	-0.019
Sgrs	0.005	0.000	0.000	2.736	0.209	0.028	1.000	0.000	0.012
Sphl	-0.022	-0.002	0.000	81.858	6.249	0.838	1.000	0.000	0.359
Seas	-0.152	-0.012	-0.002	554.905	42.364	5.682	1.000	-0.001	2.433
Sann	-0.148	-0.011	-0.002	539.286	41.171	5.522	1.000	-0.001	2.365
Smnb	-0.001	0.000	0.000	4.620	0.353	0.047	10.000	0.000	0.203
Sms	0.180	0.014	0.002	-655.854	-50.071	-6.716	1.000	0.001	-2.876
Scel	0.093	0.007	0.001	-339.885	-25.948	-3.480	1.000	0.000	-1.491
Sfec	0.051	0.004	0.001	-184.929	-14.118	-1.894	1.000	0.000	-0.811
Spg	1.495	0.114	0.015	803.434	61.337	8.227	1.000	0.007	3.523
Scch	1.207	0.092	0.012	-85.925	-6.560	-0.880	1.000	0.005	-0.377
Same	0.186	0.014	0.002	-13.232	-1.010	-0.135	1.000	0.001	-0.058
Sdap	1.583	0.121	0.016	-112.766	-8.609	-1.155	1.000	0.007	-0.495
Smnc	0.002	0.000	0.000	-0.167	-0.013	-0.002	10.000	0.000	-0.007
Sczo	0.000	0.000	0.000	0.000	0.000	0.000	1.000	0.000	0.000
Sab	-1.495	-0.114	-0.015	-803.434	-61.337	-8.227	1.000	-0.007	-3.523
San	-0.015	-0.001	0.000	-8.209	-0.627	-0.084	1.000	0.000	-0.036
Sqtz	5.001	0.382	0.051	3126.035	238.654	32.010	1.000	0.022	13.709
Swater	-13.408	-1.024	-0.137	44.927	3.430	0.460	1.000	-0.059	0.197
Vprp	153.681	-3.778	-22.134	12604.665	-309.884	-1815.403	0.100	0.082	6.724
Valm	177.971	-4.375	-25.632	20555.013	-505.342	-2960.461	0.100	0.095	10.965
Vsps	0.187	-0.005	-0.027	308.039	-7.573	-44.366	0.100	0.000	0.164
Vgrs	-0.361	0.009	0.052	-194.144	4.773	27.962	0.100	0.000	-0.104
Vphl	1.591	-0.039	-0.229	-5808.048	142.790	836.511	0.100	0.001	-3.098
Veas	10.785	-0.265	-1.553	-39373.153	967.983	5670.767	0.100	0.006	-21.003
Vann	10.482	-0.258	-1.510	-38264.857	940.736	5511.144	0.100	0.006	-20.412
Vmnb	0.090	-0.002	-0.013	-327.777	8.058	47.208	1.000	0.000	-1.748
Vms	-12.748	0.313	1.836	46536.656	-1144.097	-6702.500	0.100	-0.007	24.824
Vcel	-6.606	0.162	0.951	24115.953	-592.887	-3473.330	0.100	-0.004	12.864
Vfec	-3.594	0.088	0.518	13121.222	-322.583	-1889.800	0.100	-0.002	6.999
Vpg	-106.112	2.609	15.283	-57009.635	1401.573	8210.884	0.100	-0.057	-30.411
Vcch	-85.609	2.105	12.330	6096.574	-149.883	-878.067	0.100	-0.046	3.252
Vame	-13.183	0.324	1.899	938.850	-23.081	-135.219	0.100	-0.007	0.501
Vdap	-112.352	2.762	16.182	8001.058	-196.705	-1152.362	0.100	-0.060	4.268
Vmnc	-0.166	0.004	0.024	11.843	-0.291	-1.706	1.000	-0.001	0.063
Vczo	0.000	0.000	0.000	0.000	0.000	0.000	0.100	0.000	0.000
Vab	106.112	-2.609	-15.283	57009.635	-1401.573	-8210.884	0.100	0.057	30.411
Van	1.084	-0.027	-0.156	582.433	-14.319	-83.886	0.100	0.001	0.311
Vqtz	-355.247	8.734	51.165	-222040.091	5458.821	31979.600	0.100	-0.189	-118.442

ΔXrp:	0.004
ΔXalm	0.009
ΔXgrs	-0.012
ΔT(K)	4.165
ΔP(bar)	359.486

Table 8-1. Partial derivatives for the error estimation in the biotite-bearing system (F2205).

The correlation coefficients (ρ) were determined using Monte Carlo procedure. The chemical composition data were randomly perturbed within their standard error for more than 200 times, so that the resulting errors in the calculated end-member compositions were estimated. It is confirmed by Kohn and Spear (1991) that the Monte Carlo procedure provides reasonable error estimates.

The uncertainties for the initial temperature and pressure were set to 25 °C and 500 bars, respectively, according to the literature (Ferry, 1980; Kohn, 1993). Initial mineral compositions were assumed to have large errors. Uncertainties of 10 % relative to the input values were used for chlorite and biotite, except for their Mn end-members for which relative uncertainties of 20 % were assumed. 5 % (relative to their value) were used for other minerals. Almandine, albite, and paragonite contents are generally high and do not fluctuate largely, therefore 5 % of uncertainty may be overestimating. Errors of 2 % (relative to their value) were given for them. Changes of garnet compositions, namely the monitor parameters, were assumed to have 5 % of uncertainties relative to their value. Uncertainties in entropy data were assumed to be ±1 J/mol K, though ±10 J/mol K was applied for Mn-chlorite and Mn-biotite. Uncertainties in molar volume data were assumed to be ±0.1 J/bar, and again ±1 J/bar was used for Mn-chlorite and Mn-biotite.

The propagated uncertainties due to the input initial conditions and the monitor parameters for a chosen step in sample F2205 ($\Delta T = 4.2°C, \Delta P = 360$ bar) of biotite-bearing system were 0.56 °C and 140 bar (1σ). For the biotite-free system, the propagated uncertainties for the chosen step in sample F1401 ($\Delta T = 3.9°C, \Delta P = 240$ bar) was 0.50 °C and 31 bar (fig.8-8).

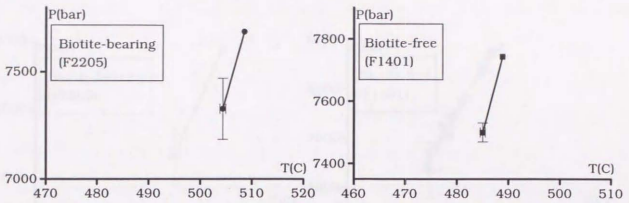

Fig.8-8. Propagated errors due to the input data for the representative steps of the biotite-bearing and the biotite-free systems.

The derived pressure uncertainties above seem rather large, but it must be noted that it includes the largest possible error due to the given initial condition. The uncertainty will be an order of magnitude smaller for the calculation of the other steps of the grain. It is because the uncertainties for the other steps only account for that of counting statistics, which are about 1/10 to 1/5 of the uncertainties in the initial conditions. If 1/5 of the initial uncertainties were assumed for the mineral compositions, the uncertainties arising from the counting statistics for the whole calculated P-T path of the sample F2205 were about 1.5°C and 280 bar. Those for the whole path of the sample F1401 were 10°C and 540 bar.

Thus the estimated total uncertainties for the five calculation steps with the biotite-bearing system in the sample F2205 were on the order of 2.1°C and 420 bar for the total history of 18.4°C and 1540 bar. The finer the calculation step, the less uncertainty expected. The total P-T change derived from the biotite-free sample, F1401, were 58.0°C and 2570 bar, whereto the

propagated uncertainties were on the order of 11 °C and 570 bar (fig.8-9).

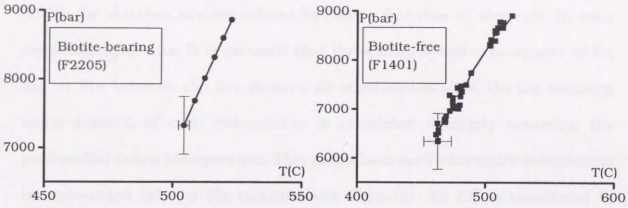

Fig.8-9. Total propagated errors for the whole P-T paths.

8-4. Activity-composition relationships of chlorite and biotite

Proposed activity models for these two minerals (e.g., Holland et al. (1998) for chlorite) are formulated by molar fractions of elements in each crystallographic site. It is assumed that there is no selective occupancy of Fe, Mg, or Mn between the two distinct six-coordination sites. On the contrary, molar fraction of each end-member is calculated definitely assuming the preferential cation incorporation. This arises because Tschermak's substitution is represented only by Mg end-members (fig.8-10). All Al^{VI} is considered to correspond to Mg end-members. This model will not be valid when much Al^{VI} "and" Fe are contained in the mineral. In fact, there are regions that the content of particular end-member is zero but its activity is still positive. This problem would not arise if appropriate end-members were chosen to cover the composition range. Unfortunately, it is not always possible to choose a preferable set of end-members, because of the lack of the published data of mineral thermodynamic properties.

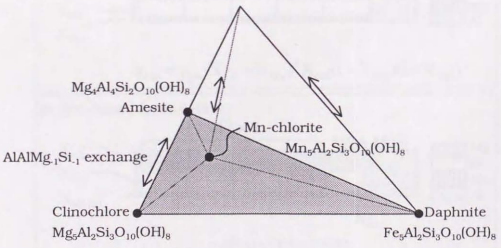

Fig.8-10. Chlorite end-members used in the calculation.

To avoid the problem, calculations of molar fractions and activities must use the same assumption for the distribution of Mg, Fe, and Mn. One way is to formulate the molar fractions of elements on certain site using end-member contents. It means selective incorporation of elements between different sites must be assumed (fig.8-11a). This end-member-based approach was applied in the previous chapters.

Another model is to calculate the activities, and the molar fractions of the end-members, based on the cationic molar fraction on each site (fig.8-11b). If no selective incorporation occurs, as assumed in this model, total Al^{VI} corresponds to all Mg, Fe, and Mn end-members. However in the calculation, the Al^{VI} must be treated as Mg end-members (eastonite and amesite).

Calculations were carried out using the two different activity formulations (Table 8-2, Fig.8-12). It is obtained that the results for the same

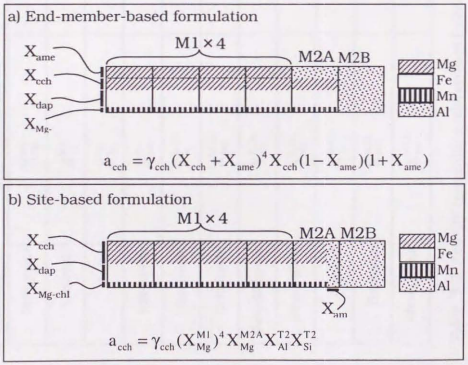

Fig.8-11. Two approaches for the calculation of the activities in chlorite. The same approaches were applied to biotite.

End-member	Mole fraction (Xi)	Activity (ideal part)	Activity (nonideal part)
Phlogopite	X_{Mg}^{M1}	$4\left(X_{Mg}^{M2}\right)^2 X_{Mg}^{M1} X_{Al}^{T1} X_{Si}^{T1}$	Symmetric regular solution model, W from Holland and Powell (web)
Eastonite	X_{Al}^{M1}	$\left(X_{Mg}^{M2}\right)^2 X_{Al}^{M1} \left(X_{Al}^{T1}\right)^2$	
Annite	X_{Fe}^{M1}	$4\left(X_{Fe}^{M2}\right)^2 X_{Fe}^{M1} X_{Al}^{T1} X_{Si}^{T1}$	
Mn-biotite	X_{Mn}^{M1}	$4\left(X_{Mn}^{M2}\right)^2 X_{Mn}^{M1} X_{Al}^{T1} X_{Si}^{T1}$	
Muscovite	X_{Al}^{M2A}	$4 X_{Al}^{M2A} X_{Al}^{T1} X_{Si}^{T1}$	Ideal mixing
Celadonite	X_{Mg}^{M2A}	$\left(X_{Mg}^{M2A}\right)\left(X_{Si}^{T1}\right)^2$	
Fe-celadonite	X_{Fe}^{M2A}	$\left(X_{Fe}^{M2A}\right)\left(X_{Si}^{T1}\right)^2$	
Clinochlore	X_{Mg}^{M2A}	$4\left(X_{Mg}^{M1}\right)^4 X_{Mg}^{M2A} X_{Al}^{T2} X_{Si}^{T2}$	Symmetric regular solution model, W from Holland and Powell (web)
Amesite	X_{Al}^{M2A}	$\left(X_{Mg}^{M1}\right)^4 X_{Al}^{M2} \left(X_{Al}^{T2}\right)^2$	
Daphnite	X_{Fe}^{M2A}	$4\left(X_{Fe}^{M1}\right)^4 X_{Fe}^{M2A} X_{Al}^{T2} X_{Si}^{T2}$	
Mn-chlorite	X_{Mn}^{M2A}	$4\left(X_{Mn}^{M1}\right)^4 X_{Mn}^{M2A} X_{Al}^{T2} X_{Si}^{T2}$	

Table 8-2. Activity-composition relationships based on the molar fractions of cations on the crystallographic sites. Resulting activities for muscovite are equivalent to those from the end-member-based model.

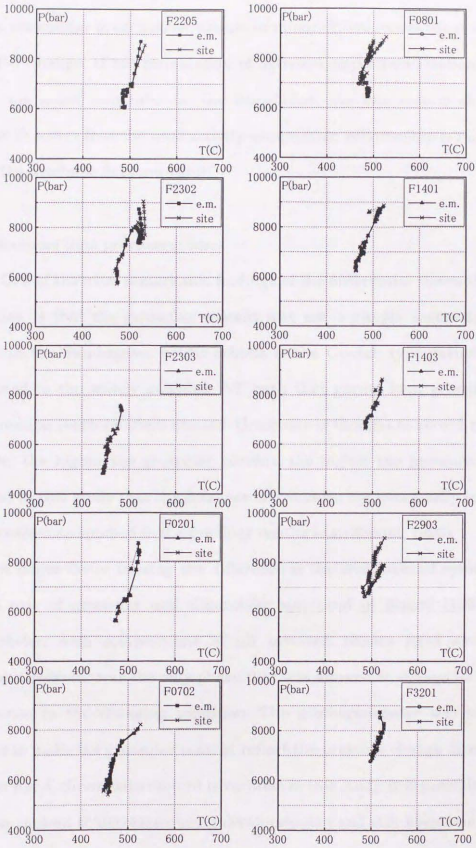

Fig.8-12. Comparison of calculated P-T paths using different activity models for biotite and chlorite. "e.m." represents the calculations using the models based on the molar fractions of end-members. "site" represents those based on the cation content on each site.

samples are similar to each other, except for minor differences in the magnitude of the P-T change. If the formulation of activity-composition relationships is putting too much constraint on the calculation, the two results should be different. It seems that the used activity-composition relationship is reliable as long as the available data are valid.

8-5. Differences from previous studies

One of the most remarkable findings of the differential thermodynamic calculation is that the grossular content was not a simple barometer. Most popular in the Sambagawa pelitic schists is the Ca-rich type garnet, which contributed to the widely accepted P-T path that garnet kept growing after decompression (=exhumation) started. Grossular is thought to record pressure condition, the higher the grossular content, the higher the pressure. It was found out in this study that the decrease of grossular not necessarily indicated decompression as opposed to the previous results (e.g., Enami, 1998).

A major factor causing the difference is the treatment of epidote. The mineral pair of grossular and clinozoisite was used in Enami (1998) as a geobarometer, with compositions of all involved phases fixed except for grossular. Grossular was the only phase that was allowed to change its content in response to the changing condition. The geothermometer was virtually designed to make the grossular content reflect the pressure change directly. On the other hand, clinozoisite content is variable in this study. It is possible for the grossular content to decrease during decompression and still keep equilibrium with clinozoisite, if the activity of clinozoisite also decreases simultaneously.

It is clear that different P-T paths are worked out depending on

calculation models. Judging from the consistency of the calculated results on anorthite and clinozoisite content, the differential thermodynamic method seems reliable about the behavior of Ca in the supposed systems. Besides, the model in this study involves almost the whole system of the metamorphic rocks, which had not been done before for the Sambagawa belt. It is suggested that the differential thermodynamic method is more appropriate to calculate the behavior of the total system. The great advantage of the calculation in this study is that it has been constructed to be a neutral model. Nothing had been assumed in advance regarding to whether grossular component reflects pressure or not.

There are still other evidences that indicate pressure decrease for the last recorded stage. Higashino (1975) examined the dissolution texture of garnet into biotite and pointed out that biotite formation required a decrease of pressure. Enami (1994) calculated the dP/dT using chemical zoning of Na-pyroxene in quartz schists assuming they were in equilibrium with garnet. The derived values were 3.2 kbar/100°C (9 – 10°C/km) for the chlorite zone, but – 1.8 to 0.4 kbar/100°C for the garnet and the albite-biotite zones. The latter case is thought to indicate reheating during exhumation. In both cases, however, it is not certain that the decompression occurred simultaneously with heating. Now that garnet does not record decompression history during heating, it is more likely that those evidences were produced at some other time, namely the retrograde stage.

Zoning patterns of garnet with complicated Mn behaviors have been reported from several areas of the Sambagawa belt. Some are interpreted to have detrital origin, for they exhibited cores with different composition and

irregular but angular shape (Higashino and Takasu, 1982). Others are regarded as indicating decompression, since the Mn fluctuation occurred at the outer portion of the grain conformably (Nomizo, 1993). Ca behavior in those cases is not uniform.

The composite zoning examined in this study is similar to those reported by Takasu (1986) from the pelitic schists at the boundary against the Sebadani metagabbro mass. The grains exhibit two times of normal zoning, and the euhedral growth surfaces of the earlier growth are truncated by the resorption texture. The chemical trend described by Takasu (1986) has no decrease of Mg/Fe ratio during the resorption. On the contrary, Mg/Fe ratios in the composite zoning in this study commonly decrease after the resorption stage, which derive the results of cooling. Takasu (1986) interpreted that the later growth of garnet occurred only when the temperature reached higher than that at the time when the existing garnet was finally formed. This study showed, however, that it was not necessarily hotter than before when the later growth started.

The difference was presumably caused by the difference in the extent of resorption, which most likely disturbed the outermost rim of the first growth. Suppose substantial amount of garnet was resorbed at the time interval, it is possible from the law of mass balance that garnet grains started to form at lower temperature than they finally experienced.

If there were enough reactant materials for garnet in the matrix, even a small temperature increase will cause a large overstepping. It may lead to a rapid garnet growth. It is possible that the very high Mn content at the beginning of the later growth was kinetically controlled, since Mn has too

strong a tendency to be incorporated into garnet. If this is true, the extremely Mn-rich portion at the beginning of the later growth is not suitable to treat assuming equilibrium. The large pressure decrease calculated from the sample F2903 should be an artifact. It is speculated that the extremely Mn-rich part was formed by the same mechanism that formed the minor non-equilibrium growth at the outermost rim and sector zoning in garnet. It is also possible that grains with sector zoning were also created at the beginning of the later growth, but were resorbed during the resorption stage.

The P-T path of F2302 shows minor decrease of pressure halfway. Mg/Fe ratio shows minor decrease near the rim of garnet in this sample. Grossular content also decreases associated with the Mg/Fe ratio, which is responsible for the deviation of the P-T path. Decrease of the Mg/Fe ratio means that this sample should be identified as the composite zoning, though there is no resorption texture or the characteristic increase of spessartine generally observed at the beginning of the later growth in the composite zoning. Garnet in sample F2302 has substantial resorption texture at the outermost rim and it is difficult to determine the detailed behavior of chemical elements toward the rim. Analyses of more samples will be required to determine whether the zoning pattern of F2302 is the result of the modification after the peak condition, or it should be identified as another type of zoning pattern in the area.